SERS-ACTIVE NYLON FIBER EVIDENCE SWABS FOR FORENSIC APPLICATIONS

A thesis presented to the faculty of the Graduate School of
Western Carolina University in partial fulfillment of the
requirements for the degree of Master of Science in Chemistry.

By

Matthew Darren Burleson

Director: Dr. David D. Evanoff, Jr.
Associate Professor of Chemistry
Department of Chemistry & Physics

Committee Members: Mrs. Brittania J. Bintz, Forensic Science
Dr. Channa R. De Silva, Chemistry
Dr. Kelly S. Grisedale, Forensic Science
Dr. Scott W. Huffman, Chemistry

June 2016

ACKNOWLEDGEMENTS

First and foremost I would like to thank my research advisor, Dr. Evanoff, for his expert guidance, zealous attitude towards my project, and his patience throughout the project. The invaluable experience I have gained under his guidance will forever be with me and continue to influence me as a chemist. I would also like to thank my committee members for their willingness to be my committee and their expert guidance as well, and their tips for improvement when asked. I would like to thank Dr. Vinay for his aid in the project and his helpfulness in all aspects of his involvement. I would like to thank the department in general not only for the education I've received here, but the encouragement from the department as a whole. I would also like to thank the Clemson University Electron Microscope Facility for providing access to electron microscopy for images. Lastly, I would like to thank the National Institute of Justice for helping to fund this project (2015-NE-BX-K003) and also the National Science Foundation (CHE-1040163) for providing funding for the essential instrumentation.

I also would like to thank my friends and family who have supported me along this journey. Specifically my dad, I can't extend my gratitude enough for his ensuring that I achieved my degrees. I also want to thank Nicole Dragan for being supportive of me and my work and being the most amazing study partner anyone could ask for.

TABLE OF CONTENTS

LIST OF TABLES

LIST OF FIGURES

LIST OF ABBREVIATIONS

$[Ru(bpy)_3]^{2+}$ .....tris(2,2'-bipyridyl)ruthenium(II) chloride

AP .....acid phosphatase

Arb. u. .....arbitrary units

CCD .....charge-coupled device

CV .....crystal violet

ICP- OES .....inductively coupled plasma optical emission spectrometer

IRI .....integrated Raman intensity

Lp .....laser power

NDF.....neutral density filter

NPs.....nanoparticles

PBS .....phosphate-buffered saline

PDDA.....poly(dimethyldiallylammonium chloride)

PIC .....picroindigo carmine

PSA .....prostate specific antigen

RRS.....resonance Raman scattering

SAP .....seminal acid phosphatase

SEM .....scanning electron microscopy

SERRS .....surface enhanced resonance Raman scattering

SERS.....surface enhanced Raman scattering

SPH .....spermine phosphate hexahydrate

UV-Vis .....ultraviolet-visible spectroscopy

ABSTRACT

SERS-ACTIVE NYLON EVIDENTARY SWABS FOR FORENSIC APPLICATIONS

Matthew Darren Burleson, M.S.

Western Carolina University (June 2016)

Director: Dr. David D. Evanoff, Jr., Ph.D.

In the field of forensic science, discovered materials that could potentially be used as evidence are screened using presumptive and confirmatory tests before the samples are subjected to DNA analysis. Both of these tests have drawbacks associated with their use, such as being prone to false positive and negatives. Only one biological fluid can be analyzed using one of these tests at a time. Further, these tests are destructive to the sample, meaning no further analyses could be performed on the same sample portion. Herein, we report the functionalization of commercially available nylon evidentiary swabs to serve as a SERS-active medium for non-destructive confirmatory analysis of seminal fluid by attaching silver nanoparticles grown via the hydrogen reduction method to the fibers. The resulting swabs have been analyzed using inductively coupled plasma optical emission spectroscopy (ICP-OES) and electron microscopy to assess the silver nanoparticle coverage. The two model dye compounds crystal violet and tris(2,2'-bipyridyl)ruthenium(II) chloride were analyzed using SERS as a proof of concept and examination of SERS enhancements, respectively. The research includes the study of the effects of swab fabrication on surface coverage, particle size and spacing, and Raman and SERS spectral enhancement of the two model dyes and seminal fluid. Efforts to maximize seminal fluid SERS signal while exploring the effect of swab storage is also presented.

CHAPTER 1. BACKGROUND

1.1. Introduction to current evidence screening techniques

Bodily fluids found at crime scenes are among the most important pieces of evidence in a forensic investigation.[1,2] These fluids may include, but are not limited to, blood, semen and saliva and can be collected at the crime scene using swabs.[2] These swabs can be made of cotton, nylon and rayon materials.[3] Cotton swabs are the most commonly used swabs in forensic casework. Unlike nylon swabs, cotton swabs do not have their fibers flocked, that is, arranged in a perpendicular fashion, but rather in a mattress design which is a result of the cotton being wound tightly around the shaft material, forming the swab tip.[3] This design results in a dense inner core of cotton that can trap the evidentiary materials.[3] Biological fluid is often important evidence since it can often prove a crime was committed, potentially identify a suspect, and exonerate an innocent person. For example, semen can be used to prove that intercourse occurred. Identification of a bodily fluid, and subsequent speciation of the donor of the fluid is performed using screening tests. The type of test used depends on what bodily fluid is suspected to be present. The tests subsequently explored will be for the possible presence of seminal fluid, biological fluid that may contain spermatozoa.

1.1.1. Presumptive screening tests

Presumptive tests are used to establish a possibility that a bodily fluid or tissue is present.[2] The most widely used and validated presumptive test for the detection of seminal fluid is the seminal acid phosphatase (SAP) test which identifies the enzyme acid phosphatase (AP).[2,4] Acid phosphatase refers to a class of enzymes found in nature and animals but is secreted into seminal fluid by the prostate gland.[4,5] AP is also found in other bodily fluids including blood,

saliva, urine, vaginal secretions and other fluids, however the amount of AP in seminal fluid is about 400 greater than in the aforementioned fluids.[4,5] Because all these sources can produce AP, and could even produce a false positive result, these tests cannot be used specifically to determine what bodily fluid may be present. This then requires other testing methods to be used for confirmation.[4] Forensic laboratories commonly use the Brentamine spot test as the SAP screening tool.[4] With this test, the enzyme AP is used to catalyze the hydrolysis of organic phosphate, alpha-naphthyl phosphate. This organic phosphate serves as the substrate that reacts with AP, forming a product that produces a purple color change, which indicates the potential presence of semen when reacted with a diazonium salt chromogen, Brentamine Fast Blue dye.[6] This test is sensitive enough that a positive result could be yielded even with semen diluted 500 times.[7] The rate at which the color change occurs can also be used to indicate the possible presence of semen.[5] Typically, reaction times of less than 30 seconds are considered to be indications of the presence of semen.[5] These tests cannot be used specifically to state what bodily fluid may be present since several bodily fluids including blood, vaginal secretions and even juice from a cauliflower stem can produce a false positive outcome and why other testing methods must be used for confirmation.[4,7]

1.1.2. Confirmatory screening tests

Confirmatory detection of spermatozoa cells is done using microscopy and confirms the species of origin is human.[2] Treating the sperm cells with established staining techniques allows the cells to be viewed and distinguishable from extraneous material, such as vaginal epithelial cells, when viewed under a microscope.[7,8] The most popular stain used is the Christmas tree stain, in which picroindigocarmine (PIC) stains the neck and tails of the spermatozoa green, and

Nuclear Fast Red gives the head a red color and the cap a pink color.[2] Different mammals will have different sperm cell morphology that the examiner must be trained to distinguish.[7]

The prostate-specific antigen (PSA) test is another example of a confirmatory analysis technique that enables detection of the protein p30, or PSA.[2,5] This protein is distinctive to human seminal plasma allowing its detection to be considered confirmatory.[2,5] Azoospermic males, males with no sperm count, will also have the antigen in their seminal plasma.[2] PSA is present in other bodily fluids but below a detectable limit compared to seminal plasma, so they do not interfere with results.[2]

Several problems are associated with both presumptive and confirmatory tests. Both testing methods can be expensive requiring the purchase of additional equipment and are time consuming. Additionally, each test is designed to detect one bodily fluid, which means testing for mixtures becomes a problem, as only one of the present fluids would be detected. Additionally, the tests are also destructive to the portion of sample analyzed.[2] Sample destruction is a potential issue in forensic analyses since evidence samples are often limited, but contain information that is critical to an investigation. Introducing novel evidentiary screening techniques like Raman spectroscopy into the forensic workflow process could have the capacity to reduce the impact of the problems associated with the current screening techniques.

1.2. Raman spectroscopy

Radiation interacting with samples can undergo many processes such as absorption, reflectance, transmission and scattering.[9] When this scattered radiation has the same frequency as the incident radiation, or is elastically scattered, it is termed Rayleigh scattering.[9] Conversely, if the scattered radiation experiences a shift in frequency, or is inelastically scattered, it is termed Raman scattering.[9] Both forms of scattering involve the momentary excitation of an electron

from the ground state to a virtual state, and the re-emission of radiation as the molecule relaxes from this virtual state, a short lived quantum state, as shown in Figure 1.[10,11] When the scattered radiation has shifted to a lower frequency it is called stokes Raman radiation, and scattered radiation that is higher in energy is called anti-stokes Raman radiation.[12]

Raman scattering is the basis of Raman spectroscopy, a non-destructive vibrational spectroscopic technique. Raman spectroscopy examines the inelastic scattering of monochromatic light by analyte molecules as the scattered photons have an energy which corresponds to a change in quantized energy levels of molecules.[9] As a technique, Raman spectroscopy is used to examine vibrational, rotational and other transitions in molecules. Additionally, Raman spectroscopy can be used to identify the functional groups of biological molecules, because these molecules will have different interactions with light, giving rise to distinctive spectral bands which produce a unique "spectral fingerprint."[13]

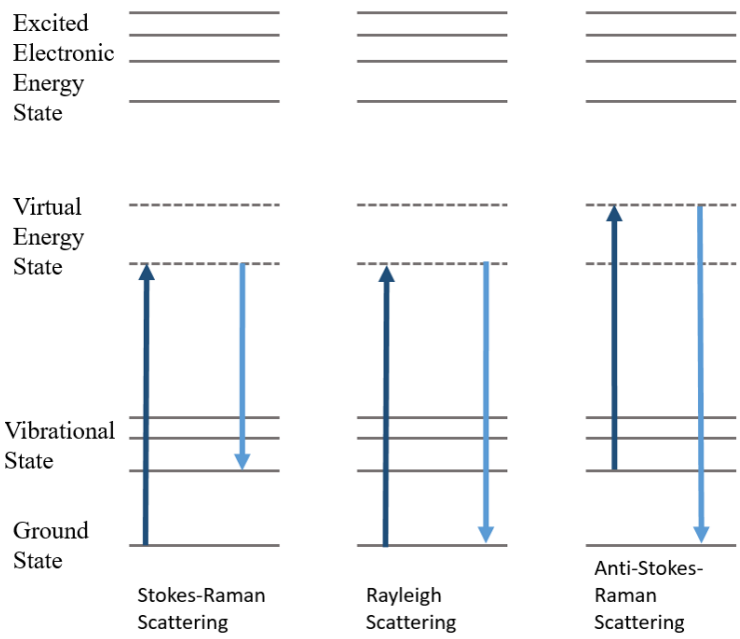

Figure 1. Jablonski diagram showing the Raman scattering vs. Rayleigh scattering processes.

For a molecular vibration to be Raman-active and detectable using Raman spectroscopy, the polarizability of the analyte molecule must be considered. Polarizability refers to the deformability of the electron cloud around the analyte molecule by an external electric field, causing an induced dipole.[10] A Raman-active vibration will experience a change in polarizability over the course of the vibration.[9] Due to this selection rule, the potential use of Raman for the investigation of biological fluids is considerable, as water will not interfere. Water can be an interferent in another type of vibrational spectroscopy more commonly found in crime labs, infrared (IR) spectroscopy.

Raman scattering typically has a weak signal because Raman scattering is a rare event. In fact, only one in approximately 10^6 - 10^8 photons will be Raman scattered with the rest being Rayleigh scattered.[11] Because of this, difficulties arise measuring both dilute concentrations and small amounts of sample. Another problem associated with Raman scattering is that fluorescence can overwhelm the useful Raman signal. One way to overcome these limitations is to enhance the Raman signal by placing the analyte on/near a nanostructured surface of a noble metal (typically copper, gold or silver), a measurement technique referred to as surface enhanced Raman scattering (SERS). Recently, Stamplecoskie *et al.* found that silver nanoparticle size in the range of 50-60 nm provided maximum SERS enhancements.[14]

1.2.1. Raman spectroscopy in forensic science

Raman spectroscopy has seen a rise in its use in forensic applications for numerous reasons including its rapid non-destructive nature of analysis, the specificity it offers at a molecular level, and its ability to be paired to microscopes allowing for the detection of minute samples.[11] Raman spectroscopy can be used for fiber analysis, analysis of paint samples, analysis of questioned documents, identification and screening of explosives, and has recently

been shown to serve as a screening technique for liquid samples from clandestine methamphetamine labs.[7,11,15–17] Particularly with the screening of explosives, Raman is advantageous due to its ability to enable examination of materials through various container constituents.[15] Furthermore, the capability of using Raman chemical imaging to produce images of explosive material molecules on latent fingerprints allows the spectra of the explosive materials to be easily distingushable.[15] For fiber analysis, Raman is often employed for examination of both composition and pigments used to manufacture the material.[15] With examination of pigments, Raman has the advantage that little interference is observed from the binders and resins of the pigment.[18] Was-Gubala and Machnowski were able to show that Raman spectroscopy allowed differentiation between cotton and viscose fibers even when dyed with the same dye at the same or a very close concentration.[19] Hendra and Watson analyzed nylon fibers and were among the first to report the Raman spectra of the nylon they analyzed. The authors discussed the spectra in great detail highlighting that quality Raman spectra of the nylon could be obtained.[20]

Recently, Virkler and Lednev highlighted Raman's potential capability to be used for a more effective non-destructive confirmatory identification of bodily fluids.[21] The authors showed that five bodily fluids including semen, vaginal fluid, sweat, saliva and blood were differentiable from each other by comparison of their Raman spectra, but correlated with the known composition of each.[21] Further highlighting Raman's capability to be used, the authors compared Raman spectra of dry traces of human and canine semen; each showing distinctly different Raman spectroscopic signatures.[21] In addition, the authors were able to show that the laser radiation did not damage the sample highlighting Raman's non-destructive nature as an invaluable tool allowing further downstream testing of the same sample if necessary.[21]

Likewise, the authors presented assigned band information and concluded that albumin and lysozyme contribute most to the spectrum of human seminal fluid with significant contribution from tyrosine and spermine phosphate hexahydrate (SPH).[21,22] Comparing the Raman spectra of human semen with that of vaginal fluid, similarities could be seen such as lysozyme and urea bands, but still with considerable differences.[21]

1.3. Surface enhanced Raman scattering

SERS has become a powerful technique available to chemists for a variety of applications including biosensors, identification of natural dyes and trace analyses.[12,23] Though the exact mechanism of SERS is still debated today, it is believed to result from a combination of two mechanisms: the electromagnetic enhancement mechanism and the charge transfer mechanism.[11] Both of these mechanisms contribute to an increase in analyte signal and a decrease in the detection limit of analyte molecules. In the electromagnetic mechanism, enhancement occurs due to an interaction between the analyte and the electromagnetic field that extends from a nanostructured metallic surface during an optically-excited plasmon oscillation.[11,24] The electrons of the analyte interact with this extended field resulting in greater polarization of the molecule thus leading to enhancement of Raman scattering.[11] Enhancement factors (ratio of Raman cross-section to geometric cross-section) along the order of 10^3 to 10^{14} can be obtained from the electromagnetic enhancement mechanism.[25] It has been shown, however, that the greatest enhancement occurs between particles whose plasmons overlap, a region termed a 'hot spot.'[11] These exceptional spots can produce SERS enhancement factors of 10^{12} or even greater.[26]

The charge transfer mechanism involves a bond formed between the metal surface and analyte through the transfer of an electron from the metal to an unoccupied molecular orbital of

the analyte.[11] Charge transfer can also occur reversely through the transfer of an electron of the analyte to the conduction band of the metal.[26,27] This bond allows excitation through the transfer of electrons from the metal to the analyte molecule then back to the metal again.[11] Due to the increase in electron density, the molecule experiences an increase in polarizability, thereby increasing the Raman scattering signal.[11] The charge transfer mechanism provides weaker enhancement of signal in comparison to the electromagnetic mechanism, typically along the orders of 10 to 10^3.[25] This lowered enhancement occurs because it only occurs on the surface of the metal, whereas electromagnetic enhancement could occur from distances away from the surface.[11]

1.3.1. SERS in forensic science

Like conventional Raman spectroscopy, SERS has also seen an increase in its use in forensic investigations.[28] One of the biggest advantages of SERS is the quenching of fluorescence. In the case of investigations of pen inks, the SERS spectra were found to be more information-rich than standard Raman spectra due to fluorescence quenching.[28] In fiber analysis, SERS enabled differentiation of hair fiber that had been dyed and further indicated whether the dye was permanent or designed to wash out over time.[28] In addition, the authors could differentiate hairs that had been dyed with different brands of commercially available hair colorant using SERS.[28] SERS has been extensively used for the analysis of illicit drugs, with amphetamines being the most commonly examined.[28] Furthermore, the use of SERS in the investigation of stimulant amines provided increased sensitivity and enhancement of the sample signal rather than fluorescence, allowing each molecule to have distinct spectra despite possessing a similar chemical structure.[28]

Recent literature studies (such as that by Boyd *et al*.) has employed SERS for the identification of blood in forensic applications.[28,29] The authors were able to show that using silver nanoparticles as a SERS substrate along with nickel nanorods allowed the detection of miniscule amounts of blood, with dilutions up to 1:100,000, which had previously been unobtainable with conventional Raman.[29] Furthermore, the authors were also able to successfully detect blood by swabbing their SERS substrates, silicon substrates with nickel nanorods deposited onto the substrate and made SERS-active by a coating of silver nanoparticles, directly on mock evidence.[29] Lastly, the authors were also able to obtain useful Raman signal with quenched fluorescence even on fluorescent fabrics, such as cotton, using their SERS substrates.[29]

1.3.2. Resonance Raman scattering (RRS) and surface-enhanced resonance Raman scattering (SERRS)

Another enhancement of Raman signal occurs due to resonance Raman scattering (RRS). Resonance Raman scattering occurs when the frequency of excitation overlaps with the frequency of an electronic transition, an absorption band of the sample, resulting in enhancement of scattering.[11,30] Enhancements along the order of 10^3 or 10^4 are typical for resonance Raman scattering but enhancements up to 10^6 have also been reported.[11] The main obstacle of resonance Raman scattering is fluorescence, since fluorescence and resonance Raman each are a result of absorption of incident radiation.[11,30] The resonance Raman and fluorescence processes are shown in Figure 2.

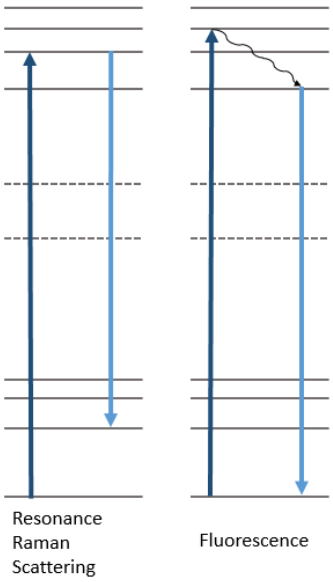

Figure 2. Jablonski diagram showing the processes of resonance Raman scattering vs. fluorescence. In fluorescence, the excited electron relaxes to a lower excited electronic energy state through an internal conversion before relaxing back to the ground state by emission of a photon. In resonance Raman scattering, the photon is scattered before an internal conversion occurs.

When SERS is used with analytes containing resonant chromophores, enhancement of the Raman signal occurs. This technique is called surface-enhanced resonance Raman scattering (SERRS). SERRS combines the advantages of SERS and resonance Raman scattering so that combinations of surface enhancement and molecular resonance enhancement are achieved.[11] SERRS can be advantageous in that fluorescence is almost completely quenched due to the chromophore being adsorbed on the surface of a SERS-active metal. This advantage allows for fluorescent materials to be measured and, additionally SERRS yields sharp bands that are specific to molecules.[11]

1.4. Introduction to the plasmonic resonance of silver

Metallic particles at the nanoscale exhibit unique properties in comparison to their bulk counterparts. An area of recent research has included the specific study of optical properties that are displayed by these nanostructures, such as surface plasmons. Surface plasmons are the

collective oscillations of free conduction electrons in response to an external electromagnetic field.[26] Surface plasmons occur in metallic particles when the wavelength of incident radiation is larger than the dimensions of the particle.[26,31] The most commonly used metals that exhibit plasmons in the visible spectral range are copper, gold, or silver.[23] Silver has numerous advantages compared to other metals including, but not limited to, its ability to support a surface plasmon across the UV-visible-NIR spectrum of 300 to 1200 nm and an interband transition occurring at higher frequencies than the surface plasmons.[31,32] Gold and copper, however, have overlap between their interband transition and plasmon resonance, thus causing the plasmons produced by gold and copper to be less efficient than those of silver.[31,32]

When an oscillating external electric field interacts with metallic nanoparticles such as silver, the metal's optical responses result from this interaction. These surface plasmons arise from the displacement of the metal's conduction electrons by acceleration from the external electric field.[31] This displacement results in an induced polarization of the particle and its surrounding material leading to the creation of a positive charge build-up at one end of the particle that decelerates the electrons, termed a restoring force.[11,31] A resonance, or sustained oscillations, occur as a result of the interplay of the incident electric field oscillation and lattice restoring force. The restoring force build-up at one end of the particle and acceleration of the electrons to the opposite end, induces polarization of the surrounding material.[11,31] Consequently, polarization of the surrounding material reduces the restoring force, shifting the plasmon resonance to a lower frequency.[31] By altering the refractive index of the surrounding medium and thus the medium's polarizability, the plasmon can be tuned to a specific position.[31]

1.5. Silver nanoparticles on fibrous materials: synthesis and applications

In addition to plasmonic properties, silver nanomaterials are known to have antimicrobial activity and as a result are commonly used in wound dressings and for coating textile materials.[33–37] Silver nanoparticles can be attached to fabrics and through this functionalization the fabric may then exhibit enhanced properties.[38–43] Montazer and Nia present one example through their research in which the authors use an *in situ* synthesis method with Tollens' reagent to synthesize silver nanoparticles on nylon fabric.[44] This process yielded an electro-conductive fabric that exhibits antibacterial properties.[44] The attachment of the silver nanoparticles also increased the tensile strength of the nylon and the increase in conductivity would allow its use in additional applications, such as electroluminescence.[44]

Meng *et al*. reported that silver nanoparticles could be grown *in situ* on silk via a UV-induced reduction method.[45] To accomplish this, they first coated silk material with a poly(acrylic acid) (PAA) and poly(dimethyldiallylammonium chloride) (PDDA) film, and subsequently soaked the silk in an aqueous solution of silver nitrate for one hour in the presence of UV radiation at 365 nm.[45] Silk is regarded for both its appearance and texture, but also provides a haven for bacteria due to its large surface area and the fact that it retains a great amount of moisture.[33] The attachment of silver nanoparticles increased the silk's antimicrobial properties as indicated by the tested inhibition zones, an area where bacterial growth has been inhibited due to the presence of the nanoparticles.[45] Increasing silk's antimicrobial ability could lead to further applications for silk in the textile industry, such as for wound dressings.

Zhang *et al*. reported another method of attaching silver nanoparticles to silk fabric.[33] The method included attaching the silver nanoparticles by dipping silk fabrics in a nanoparticle solution, rolling the fabric twice in a fabric roller, steaming for 30 minutes in a steam engine, and

finally washing with deionized water and drying.[33] By attaching silver nanoparticles to the silk, the authors were able to increase the material's antimicrobial properties as indicated by testing with *S. aureus* and *E. coli*.[33] As an example, the authors found that for an untreated silk sample versus a silver treated sample (98.65 mg/kg silver content) the surviving *S. aureus* cells reduced from 2.28×10^6 CFU/mL (colony forming units/mL) to 1.53×10^2 CFU/mL, a reduction of 99.99%.[33] Even after 50 washes of the same silver treated silk, the treated fabric still reduced the surviving *S. aureus* cells by 97.43%.[33]

Fastness measures how well the material is able to retain its properties and is often used to analyze the durability of a material through heavy use, for example, color fastness and washing fastness can be measured and reported according to standard protocol.[46] Color fastness refers to how much color is retained, and is judged on a scale of one to five with one being the most transferred.[47] Washing fastness examines how many times a material can be washed and still maintain specific properties. The color and washing fastness of silver nanoparticles attached to fabrics has been explored by many researchers. Mirjalili *et al*. studied the antimicrobial properties of silver nanoparticles attached to cellulose fabric and analyzed the fabric using a washing fastness test.[46] This test subjects the material to frequent washing and measures the durability of the nanoparticles to display antimicrobial properties while attached to the fabric.[46] Their studies showed that the silver nanoparticles were strongly attached to the fabric as indicated by the amount of bacteria reduced.[46] In fact, bacteria reduction was still at 99% even after 20 washes.[46]

CHAPTER 2. INTRODUCTION TO RESEARCH

The purpose of this research was to (1) fabricate SERS-active forensic evidence swabs by attaching silver nanoparticles to the fibers of commercially available swabs, (2) to examine the effect of swab fabrication techniques on the Raman spectral data and SERS enhancement factors of two model dye compounds, crystal violet and tris(2,2'-bipyridyl)ruthenium(II) chloride, and seminal fluid and (3) to maximize Raman signal through variation in both sampling and measurement parameters.

The first goal of this research was to outline a procedure that most effectively and reproducibly attached silver nanoparticles to the fibers of commercially available nylon swabs via the hydrogen reduction method.[48] This method utilizes ultrapure water, silver (I) oxide and hydrogen gas resulting in a matrix free from surface modifying groups during the synthesis ensuring a clean surface for investigational use of the swabs.

The second goal of the research was to examine how swab fabrication affects the Raman and SERS data obtained through the use of the swabs as a SERS-active measurement platform. To begin this process, the swabs were first studied using crystal violet as the analyte for an indication of SERS enhancement. Further studies including the limit of detection of the swabs and also how the laser power used affects the SERS spectrum were examined with tris(2,2'-ipyridyl)ruthenium(II) chloride, $[Ru(bpy)_3]^{2+}$, as the model analyte. Furthermore, seminal fluid was also examined for the same purposes and to establish the use of SERS for the non-destructive confirmatory identification of seminal fluid. The third goal of this research was to establish methods in both sampling and measurement parameters leading to maximized

Raman signal. This was first explored using the aforementioned model dye compounds and ensuring the same parameters held true for seminal fluid, as well.

The data amassed during this study will be foundational for future research projects. The examination of what affects swab uptake of biological fluid, through alterations of the synthesis could be examined. Likewise, the examination of the effect of functional groups added on the swabs' fibers on the Raman, SERS and swab zeta potential data could be studied as well. Additional work needs to be performed in order to maximize silver nanoparticle coverage on the fibers of the swabs. Additionally, a more in-depth study on synthesis times is being performed simultaneously through examination of the effects of the Raman and SERS spectral enhancements.

CHAPTER 3. EXPERIMENTAL

3.1. Materials

The nylon swabs used in this research were Copan FLOQswabs™ acquired from Life Technologies™. Silver (I) oxide (99%) was acquired from Strem Chemicals. Silver nitrate (99.9%) was acquired from Fisher Scientific. Crystal violet (99%) and tris(2,2'-bipyridyl)ruthenium(II) chloride (98%) were acquired from Acrōs Organics. Ultrapure water with a measured resistivity of 18.2 MΩ-cm was obtained from a Barnstead NANOpure Diamond system with a 0.2 μm hollow fiber filter. Hydrogen gas (research grade, 99.9995%) was acquired from Airgas. All chemicals were purchased and used without further purification. Pooled human semen (30 – 40 million cells /mL) was acquired from Lee Biosolutions. For the swabbing of dried seminal fluid from a microscope slide, the slides were sterilized via a Spectrolinker™ XL 1500 UV Crosslinker before use. Nylon supported membranes measuring 90 mm with pore size of 0.22 and 0.45 μm were purchased from Fisher Scientific. Syringe filters with nylon membranes with a diameter of 13 mm and pore size of 0.45 μm were acquired from Fisher Scientific.

3.2. Equipment and instrumentation

An open atmosphere Agilent 8453 UV-visible spectrometer was used to analyze the silver nanoparticles. A Perkin Elmer Optima 4100DV inductively coupled plasma optical emission spectrometer (ICP-OES) was used to determine silver concentrations on the fibers of the swabs preceded by a series of dilutions and filtrations as to be outlined in more detail in a subsequent section. All Raman and SERS measurements were performed using a Horiba LabRam HR Raman microscope with an 1800 groove/mm grating, an 800 mm monochromator,

and a TE-cooled charge-coupled device (CCD) detector. $[Ru(bpy)_3]^{2+}$ Raman measurements were performed using a 457.9 nm excitation from a Spectra Physics 2065-7S Ar^+ laser. The laser head power range used throughout this research was 35 – 160 mW. Neutral density filters (NDFs) were used to reduce the power of the laser at the sample to reduce damage to the swab from the laser. The NDFs affect all wavelengths the same and are on a log 10 base, for example a 1.0 NDF reduces the laser power by a factor 10. All $[Ru(bpy)_3]^{2+}$ studies utilizing a 1.0 NDF were acquired with a 1 second acquisition time and 15 accumulations. The same acquisition time was used for the 2.0 NDF but with 20 accumulations. For Raman measurements with CV, nylon and semen, a 20 mW (7.4 mW at the sample unless stated otherwise) helium-neon (HeNe) laser with a wavelength of 632.8 nm was used. The laser power was monitored using a Thor Labs, model # PM100D, meter. The objective used was a 10x infinity-corrected plan-achromat objective with a numerical aperture of 0.25. Before spectra were collected, the lasers used were aligned using a silicon standard and an acetaminophen standard was used for wavenumber calibration for semen spectra. LabSpec 6 software was used to baseline correct and smooth the Raman data. For drying, the swabs were placed inside a VAC Vacuum Atmospheres glovebox, model MO-40-2H-SSG, operating with a nitrogen environment. A Hitachi SU6600 scanning electron microscope (SEM) operating at 20 kV was used to image the nanoparticles on the fibers of the swabs.

3.3. Silver nanoparticle synthesis and swab functionalization

The silver nanoparticles used throughout this research were synthesized using the hydrogen reduction method.[48] Prior to setting up the reaction vessel, the nylon swabs had been prepared for the reaction in a two-step process. The swabs' applicator shaft was clipped to a shorter size and the remaining swab head and applicator were then soaked in ultrapure water for

24 hours to remove any impurities. Secondly, the swabs were soaked in a subsequent 48 hour soak in saturated silver (I) oxide solution to ensure the swabs' surface remains saturated during the reaction and also ensures particles form and continue to grow on the nylon fibers. The saturated silver (I) oxide solution was prepared by filtering solid silver (I) oxide out of solution using a 0.22 µm nylon filter membrane. After the 48 hour soak, 3.5 L of the saturated silver (I) oxide solution was placed into an acid cleaned 5 L Pyrex® vessel. The nylon swabs were then placed inside the reaction vessel. Silver (I) oxide (2.4 g) was then added to the reaction vessel, this amount was optimized at the beginning of the study. Heat is applied to the reaction vessel, and the temperature is monitored until it reaches 70 °C. Hydrogen gas was then applied at 10 psi above atmospheric pressure, and the vessel was vented four times to ensure a homogenous hydrogen atmosphere. The reaction was allowed to proceed for 166 minutes before being stopped. Once stopped, the swabs were removed and cleaned for future use, as per the following: the swabs were removed from the flask and rinsed with ultrapure water to remove any solid silver oxide that may have accumulated on the swab surface during extraction from the vessel. The swabs were stored in a clean container in ultrapure water before being dried for use in a glovebox. Once a swab had been used, the swab was allowed to dry on a swab drying rack at room temperature until visually dried (typically an hour). A swab that was allowed to dry during Raman measurements was allowed to visually dry on the microscope stage (typically 20 - 30 minutes).

3.4. Characterization of silver-modified nylon evidentiary swabs

For ICP-OES analysis, the swabs were prepared in the following manner: first, the applicator shaft was removed so that any silver that may have accumulated on the shaft is not analyzed. Next, the silver nanoparticles contained on the swab tips were dissolved in

concentrated nitric acid. Following this, the acid was diluted to 7% concentration with ultrapure water. Lastly, the solution was filtered using 0.45 µm nylon syringe filters.

For Raman and SERS measurements, different methods were employed to obtain Raman and SERS signal. For studies with CV solution, swab tips were soaked in the solution prior to the measurement. For studies with $[Ru(bpy)_3]^{2+}$, samples were swabbed in the following manners: solutions of $[Ru(bpy)_3]^{2+}$ were dropped into a petri dish and allowed to dry prior to swabbing. A moistened swab, wet using ultrapure water, was used to collect the dried $[Ru(bpy)_3]^{2+}$ solution. Additionally, dry swabs were also used with $[Ru(bpy)_3]^{2+}$ solutions that had not been allowed to dry for the means of examining the effects of using a wet vs. dry swab. For semen studies, the petri dish swabbing method with either a dry or wet swab was used. Further studies included swabbing semen that had been dried on a hard surface, a glass microscope slide, with a wet swab and also on a soft surface, a bed sheet, in a similar manner. Investigations of what gave the best SERS signal were investigated as well.

CHAPTER 4. RESULTS AND DISCUSSION

4.1. Silver nanoparticle synthesis and attachment to nylon fibers via the hydrogen reduction method

The hydrogen reduction method for silver nanoparticle synthesis was first outlined by Evanoff and Chumanov and allows for the synthesis of surfactant-free silver nanoparticles with control of nanoparticle size.[48] In this synthetic method, aqueous silver (I) oxide is reduced by hydrogen gas in ultrapure water by first heating the mixture to 70 °C and pressurizing the reaction vessel to 10 psi above atmospheric pressure.[48] Initially, a burst of silver nanoparticles are formed and as the reaction proceeds these initial particles continue to grow.[48] The size of the nanoparticles is controlled by altering the reaction time.[48] The simplicity of this synthesis is highlighted in the overall chemical reaction shown in Equation 1. The "chemical cleanliness" is an important aspect of this reaction as it allows further functionalization of the silver surface.

$$Ag_2O(aq) + H_2(g) \rightarrow 2Ag^0(s) + H_2O(l) \quad (1)$$

Particular to this research, the silver nanoparticles synthesized are attached to the fibers of nylon swabs. Copan FLOQswabs™ are manufactured by spraying nylon onto the tip of the applicator in the presence of an electrostatic field. As a result, they lack an inner core unlike cotton fiber swabs. Cotton fiber swabs in which the fibers are wrapped around the applicator, often contain a core which consists of dense cotton medium.[3] Evidentiary materials can be difficult to extract from these cores. The nanoparticles attach to the fibers of the nylon swabs as a result of electrostatic interaction by the donation of lone pair electrons from the nylon, a polyamide.[48,49] The donation of lone pair electrons can lower the high surface energy of the particles that results from the outermost layer being electron deficient, thus offering greater

stability.[48,49] In Figure 3 is shown two pictures of swabs after silver nanoparticles attachment for visualization of the silver-modified swabs. The 5 "lollipop" swabs shown in the left part of the picture were used initially in the research before being switched to the style shown to the right. There is no difference amongst these swabs other than the style of their tips. Precautions were taken to ensure the swabs to the right would behave the same with the synthesis.

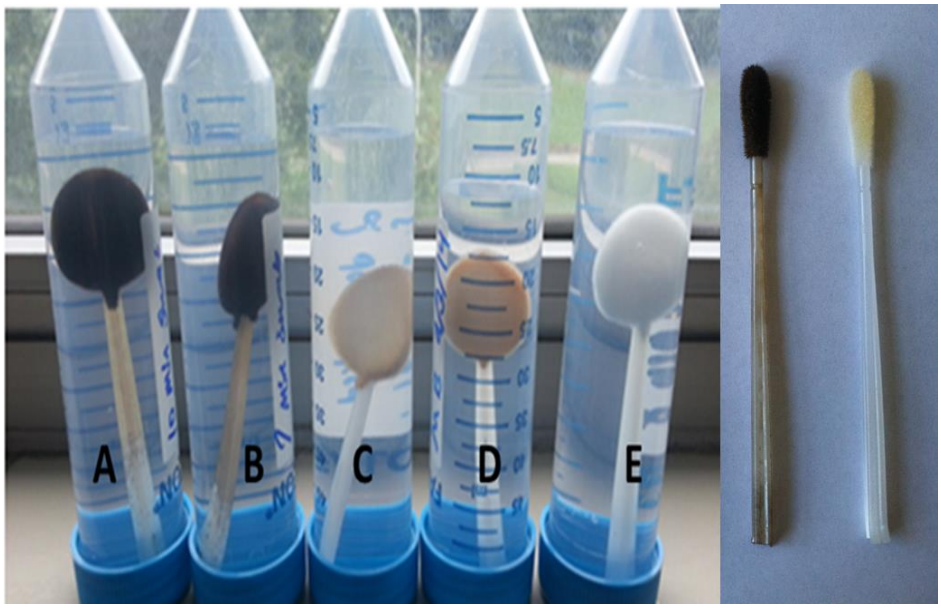

Figure 3. Nylon swabs coated with silver nanoparticles. To the left, nylon swabs coated with various concentrations of silver nanoparticles achieved by different amounts of silver (I) oxide (A) 0.32 g (B) 0.34 g (C) 0.033 g (D) 0.017 g in the reaction flask as compared to an uncoated swab (E). To the right, nylon swabs used throughout the latter part of the research.

4.2. Development of synthetic method

The first goal of this project was to develop a synthetic method for attaching silver nanoparticles to the fibers of the nylon swabs making them SERS-active. Ideally, this synthetic modification would (1) attach the nanoparticles in a reproducible and thorough manner; (2) be scalable for numerous applications; (3) allow control over the particle size and (4) provide the largest SERS enhancements possible. Initial studies of the synthetic method began by first performing the hydrogen reduction reaction with the swabs inside the Pyrex® vessel.

Initial attempts seemed to indicate that silver (I) oxide was cohering to the swabs. Based on the dark color of the reacted swabs and suspension after 1.5 hours. However, a more in-depth examination of the effect of reaction time on swab coverage was performed and showed that silver was indeed growing, but not at the typical rate of the hydrogen reduction method. To compensate for this, longer reaction times were employed and 0.22 and 0.45 µm filter membranes were used to seal the silver (I) oxide inside preventing it from adhering to the swabs. This method enabled assessment of whether the silver nanoparticles were responsible for the dark color of the swabs. In order to determine the effect of nylon in particle formation, a 0.22 µm nylon filter membrane was added to a reaction of 450 minutes. Aliquots of the suspension were taken and UV-Vis spectra were collected at timed intervals are shown in Figure 4. Spectral information allow for estimations to be deduced about the nanoparticles that were forming on the fibers of the swabs. With this in mind, it was determined that the dark color of the swabs was indeed from silver nanoparticle formation on the fibers. A second, similar reaction was run in which swabs were placed in the reaction vessel. After 166 minutes, a swab was removed and visually inspected. The amount of coverage was estimated to correlate with the darkness of the color of the reacted swabs. This swab was stored and preserved for visual comparison for future reaction schematics. All further reactions were performed for 166 minutes to reach targeted surface coverage, however, other parameters were varied to achieve homogeneity of the silver nanoparticles distribution on the swab.

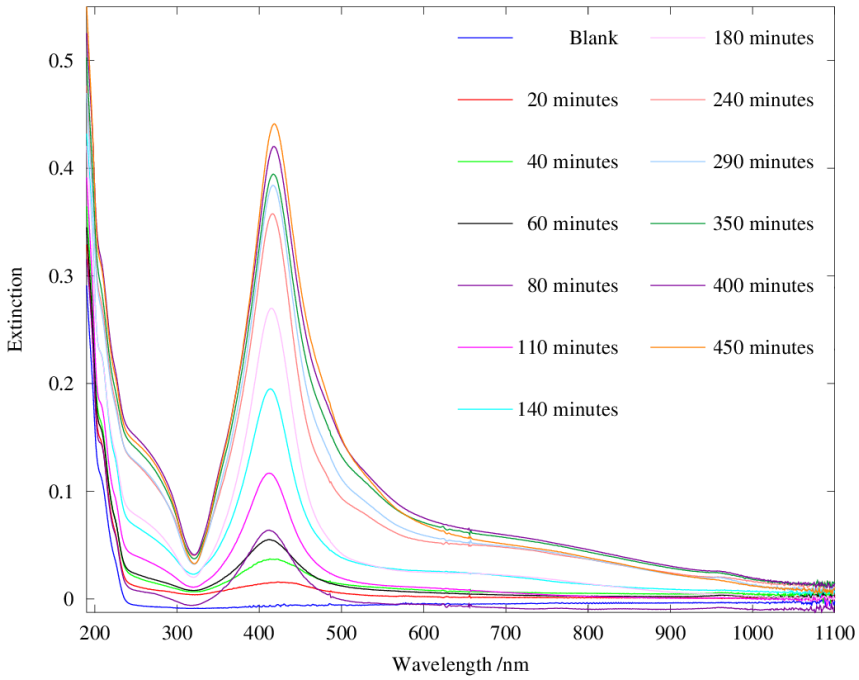

Figure 4. UV-Vis extinction spectra of nanoparticles at timed intervals up to 450 minutes.

Several studies focused on achieving more systematic coverage. First, swabs were soaked in saturated silver (I) oxide for timed intervals prior to the reaction. The resulting swabs, upon visual inspection, were more thoroughly covered when compared to previously prepared swabs. Second, solid silver (I) oxide amounts were varied in the reaction vessel along with the saturated silver (I) oxide soaked swabs, with equivalent reaction times (166 minutes). This method resulted in the most covered swabs and is the current method for silver-modified swab synthesis. Figure 5 shows the UV-Vis extinction spectrum of the silver nanoparticle suspension of two different syntheses starting with two different amounts of silver (I) oxide. A shoulder can be seen in the 2.4 g spectrum (B) highlighted by a line, that is absent in the 1.6 g spectrum (A). This shoulder indicates a small amount of polydispersity of silver nanoparticles in the

suspension. The larger amount of solid silver (I) oxide was chosen for swab nanoparticle attachment because syntheses using 2.4 grams resulted in more thorough coverage as desired.

As a test of the stability of the nanoparticles on the fibers, the swabs were stored in ultrapure water and no coloring of the water from the silver was observed. As an additional test, the swabs were sonicated in a 15 mL conical tube for time intervals of 5 – 60 minutes resulting in a slight coloration of the saturated silver oxide solution (previously made) from the silver. A UV-Vis extinction spectrum was taken to measure the presence of silver nanoparticles in the water before and after sonication and is shown in Figure 6, also shown in Figure 6 is the spectrum of the water before and after sonication of a bare non-silver modified swab. The increase in extinction observed at approximately 400 nm in the spectrum in Figure 6 (A), is attributed to leeching of the silver nanoparticles into the water. However, the spectrum indicates slight silver leeching from the swabs during the sonication demonstrating that the swabs are quite robust. In addition to the swabs containing silver nanoparticles, a bare swab was also sonicated in saturated silver (I) oxide as a control to ensure that any UV absorbing organic species coming off the swab was not reducing the silver (I) oxide to silver metal. In Figure 6 (B), there is no evidence of the characteristic extinction band near 400 nm, nor is there any evidence of organic absorbance bands in the UV.

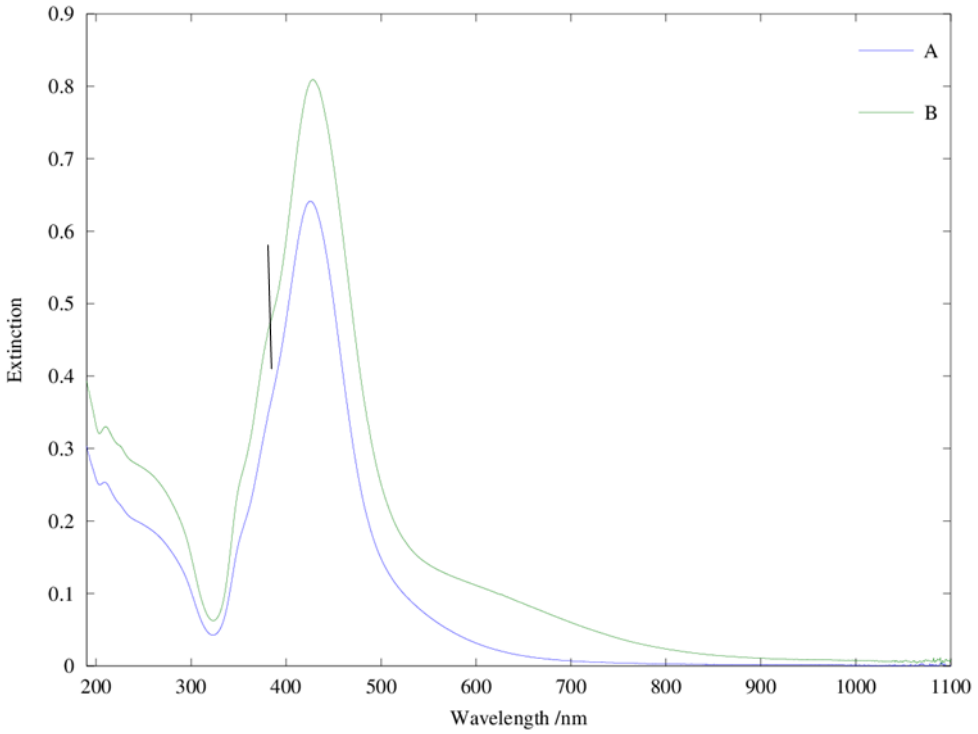

Figure 5. UV-Vis extinction spectra of silver nanoparticle suspensions (dilluted 5:1) from reactions of two different amounts of silver (I) oxide inside the reaction vessel.

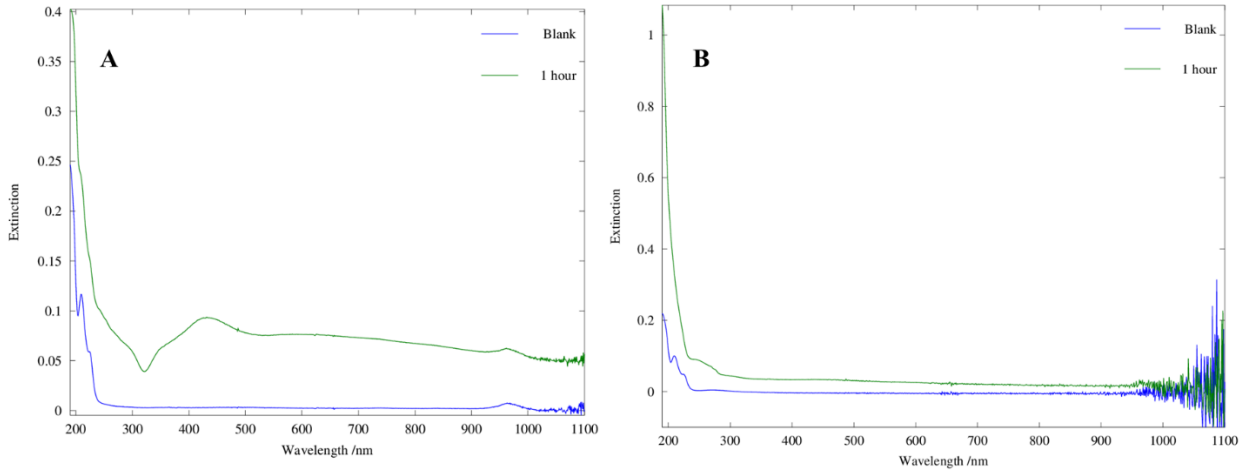

Figure 6. UV-Vis extinction spectra of (A) saturated silver (I) oxide before and after one hour of silver-modified swab tip sonication and (B) bare swab before and after one hour of sonication.

4.3. Characterization of silver nanoparticles on swabs

The silver nanoparticles attached to the swabs were characterized using ICP-OES and electron microscopy. ICP-OES analysis of the silver nanoparticles assesses the coverage on the

swabs by determining the mass of silver contained on each swab. To determine the number of nanoparticles per swab, the ICP-OES concentration was converted to mass by multiplying by the volume of solution measured. Total silver nanoparticle volume was then calculated from the mass of the silver nanoparticles per swab and the known face centered, cubic density of silver (10.5 g/cm^3).[50] The particles were assumed either hemispherical or spherical and the appropriate volume formula was used with the radius obtained from the electron microscopy measurements, yielding volume per nanoparticle. Total volume divided by volume per particle determined the number of nanoparticles contained within the total volume, as measured by ICP-OES.

Hemispherical particles were considered after visual analysis of the electron microscopy images revealed some nanoparticles were not fully spherical in geometry, therefore a range of the possible number of nanoparticles was calculated, as described above. Table 1 shows values of the average mass of silver and the calculated corresponding number of nanoparticles per swab from a single batch. This analysis was performed to determine the reproducibility of nanoparticle growth on swabs from a single batch. The data obtained indicated that silver coverage varied from swab to swab. Figure 7 shows electron microscopy images obtained of particles on fibers of the swabs. In the images, the clumps/clusters are indication of silver nanoparticles which vary in both size and location. The electron microscopy images corroborate the sporadic coverage concluded by data obtained via ICP-OES analysis. These electron microscopy images were used to obtain size information of the nanoparticles attached to the fibers. The average particle size was found to be 45 ± 14 nm (N = 112). The average particle size was determined through image analysis via Photoshop, by measuring individual particles with a custom ruler set to determine the number of pixels by measuring the scale bar on the electron microscopy images.

Combined results from ICP-OES analysis and electron microscopy images were surprising given the dark color of the swabs when noted upon visual inspection and indicates that the visual inspection may not be the best measurement of coverage. Comparison of the actual particle sizes from SEM analysis with the extinction maximum of the suspensions, reveals a similar growth rate of nanoparticle size on the swab and in suspension. One difference with the silver nanoparticle size distribution is that the nanoparticles on the swabs are polydispersed. Another difference is the rate of silver nanoparticle growth in the presence of the nylon swabs is much slower than that of the typical hydrogen reduction method.[48] Typically, reactions of approximately three hours using this method produce nanoparticles significantly closer to 100 nm.[48] The sporadic coverage of the nanoparticles on the swabs is believed to be a result of the swab tips coming in contact with one another during synthesis, preventing access to the swab fibers.

Table 1. Values of average mass and number of nanoparticles per swab from a single batch as assessed by ICP-OES analysis.

Swab	Average amount of silver per swab /mg	Number of NPs per swab ($x10^{12}$)[a]
1	0.54 ± 0.04[b]	1.07 - 2.14
2	0.36 ± 0.04	0.72 - 1.44
3	0.23 ± 0.04	0.47 - 0.93
4	0.23 ± 0.04	0.47 - 0.93
5	0.34 ± 0.04	0.68 - 1.35
Average of all 5	0.3 ± 0.1[c]	0.68 - 1.36

[a]Values indicate the minimum (assuming fully spherical particles) to maximum (assuming fully hemispherical particles) range of nanoparticles, [b]values indicate the average ± calculated uncertainty, [c]value indicates the average ± standard deviation.

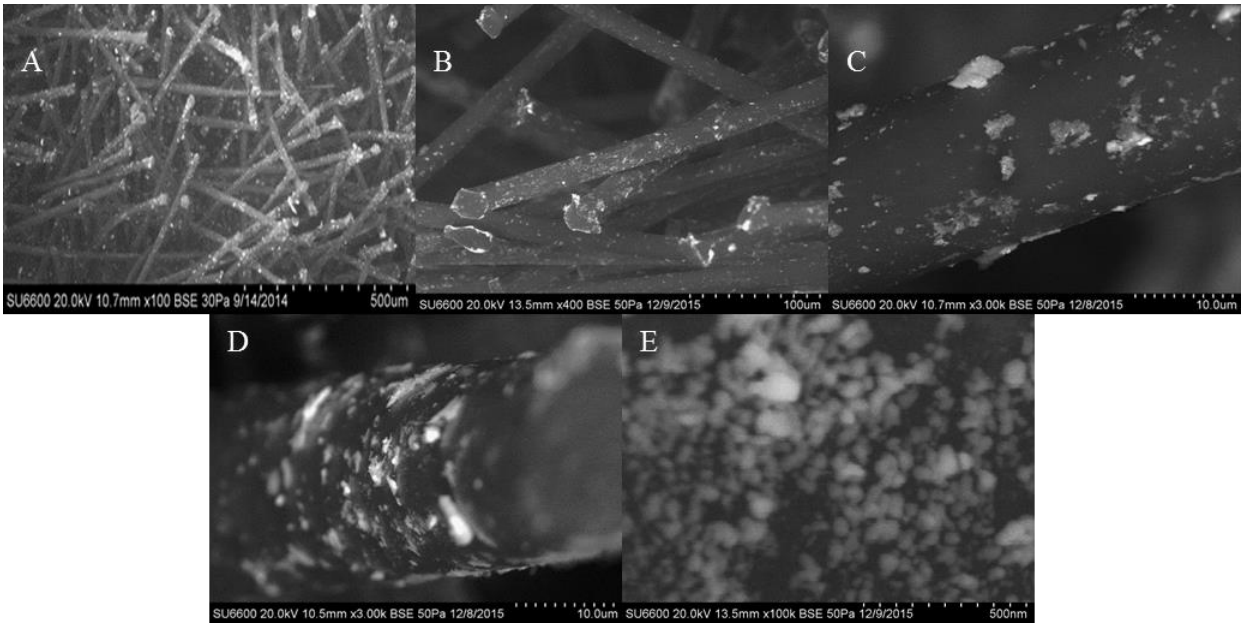

Figure 7. Electron microscopy images of silver nanoparticles on the nylon swabs. (A) image showing silver nanoparticle coverage on fibers of the lollipop style swab and (B - E) on the narrow head. Shown in (C) is a zoomed image of a single fiber whereas (D) shows an image viewed along the length the fiber of a swab. Shown in (E) is the image analyzed for particle size.

4.4. Analysis

4.4.1. Initial SERS studies – CV solution

As a proof-of-concept experiment, SERS spectra of crystal Violet (CV) solutions were successfully collected on the silver-modified swabs. Concentrations of both mM and µM were soaked onto the silver-modified swabs and analyzed. Concentrations of µM CV would not produce conventional Raman signal thus observed signal would indicate the swabs allow SERS. In Figure 8 is shown the SERS spectrum of µM CV solution obtained using a silver-modified swab (8.4 mW at the sample). The bands in the SERS spectrum not only correspond well with the conventional Raman spectrum of mM CV but also does not include Raman bands of the nylon as comparatively shown in Figure 9 in which the spectra have been normalized.

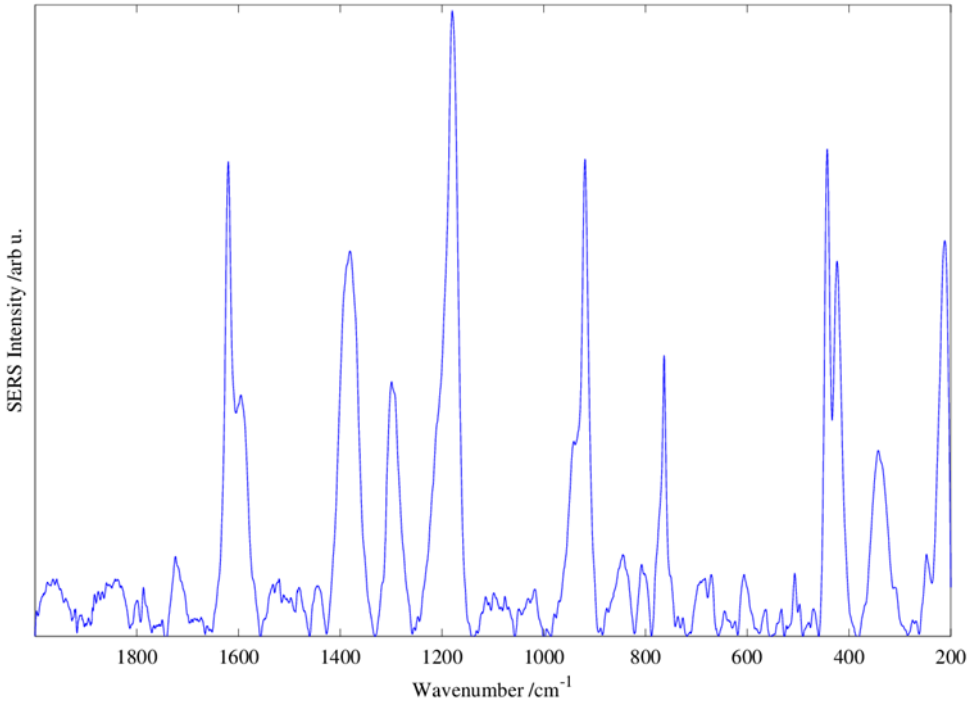

Figure 8. SERS spectrum of µM CV solution obtained through the use of a silver-modified swab.

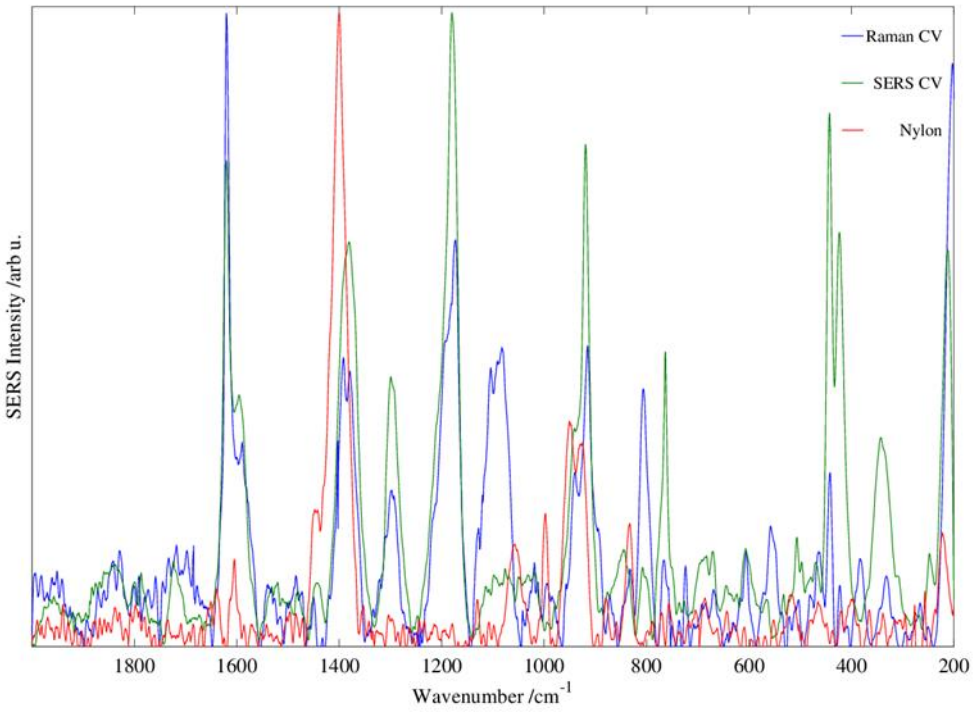

Figure 9. Comparison of crystal violet and nylon SERS spectra with the conventional Raman spectrum of CV.

4.4.2. Examination of SERS enhancement using $[Ru(bpy)_3]^{2+}$ solutions

More in-depth studies on the SERS enhancements were performed using $[Ru(bpy)_3]^{2+}$ solutions. $[Ru(bpy)_3]^{2+}$ is an exemplar choice as it produces fluorescence-quenching resonance Raman as a result of an electronic transition that overlaps well with the 457.9 nm Ar^+ laser line. Using this analyte in combination with the silver-modified swabs allows for the measurement of surface enhanced resonance Raman spectroscopy (SERRS). These studies included the determination of the SERS enhancements, determination of the limit of detection and the effect of laser power and concentration on integrated Raman intensity. In Figure 10, the raw SERS spectra of 1 x 10^{-5} M $[Ru(bpy)_3]^{2+}$ on a SERS swab using both 1.0 and 2.0 NDFs to that of a silver-less swab using the 1.0 NDF is shown. The data has not been offset. The two different measurement parameters were used to examine the spectral differences obtained with each. Only fluorescence and no Raman signal was observed across all examined power levels on the silver-less swab. The silver-modified swab, however, allows Raman signal to be detected with an improved signal-to-noise ratio, and quenches the overwhelming fluorescence. The 1490 cm^{-1} band was integrated for further studies in which the data was normalized in units by dividing by the power at the sample.

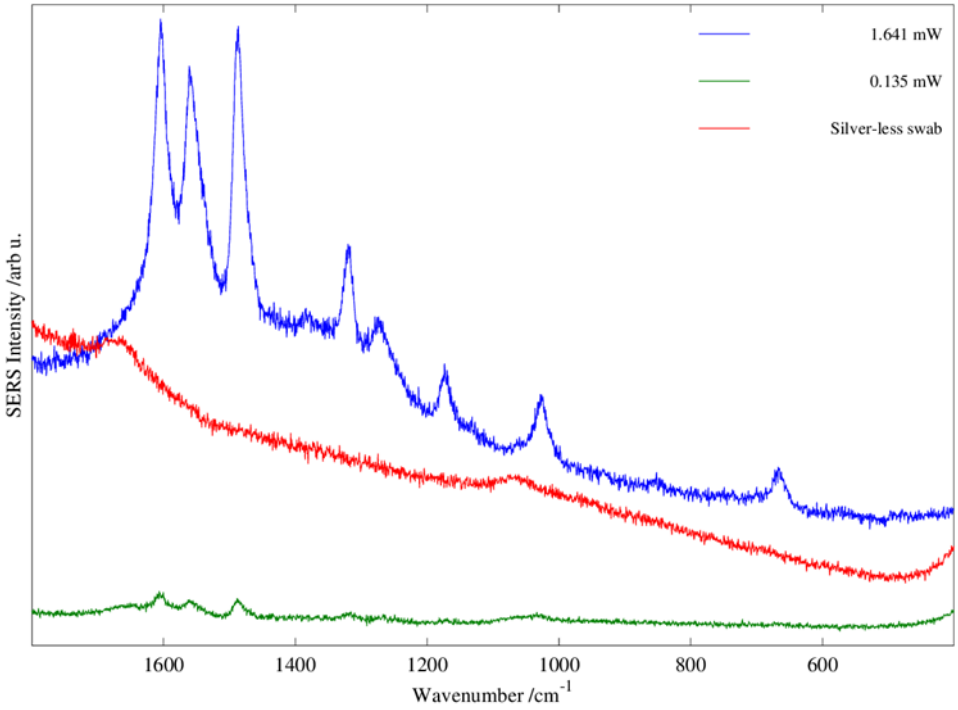

Figure 10. Comparison of $[Ru(bpy)_3]^{2+}$ signal obtained using 1.641 mW and 0.135 mW to that of a silver-less swab using 1.641 mW.

The resulting studies with $[Ru(bpy)_3]^{2+}$ are summarized in Figure 11. Shown in Figure 11 (A) is concentration vs. integrated Raman intensity (I_{RI}) in which lower concentrations resulted in increased integrated Raman intensity. This is a result of $[Ru(bpy)_3]^{2+}$ molecules being within closer proximity to the surface of the silver nanoparticles offering greater SERS enhancement. A nonlinear slope can be observed in Figure 11 (A) because there is a limit to how few analyte molecules must be present to detect greater Raman intensities, so at some concentration there would be too few molecules to produce increased integrated Raman intensities. In Figure 11 (B) is data of integrated Raman intensity as a function of laser power (*Lp*). Larger integrated Raman intensities were observed at lower laser powers as less fluorescence would have been produced during measurements. Lastly, in Figure 11 (C) is shown the SERS spectrum of 1×10^{-8} M $[Ru(bpy)_3]^{2+}$ displaying the swabs produce noteworthy SERS

enhancements. The $[Ru(bpy)_3]^{2+}$ spectrum, unlike CV, does have bands from nylon present with bands approximately at 1150 and 1400 cm^{-1}. These findings highlight that the swabs need minimum laser power for their use while simultaneously producing notable SERS enhancements. This is promising because low laser power would be less likely to cause damage to the swabs. However, it was observed during the studies with $[Ru(bpy)_3]^{2+}$ that allowing lower concentrations, such as μM, to dry and then attempting to measure resulted in difficulty obtaining SERS signal. This could result from the low population of $[Ru(bpy)_3]^{2+}$ molecules aggregating as the solution dries, and the drying causing movement of the crystals away from the silver nanoparticles which are already sporadic in location as shown in the electron microscopy images. This movement of the $[Ru(bpy)_3]^{2+}$ away from the silver would increase the chances of analyzing the space between the silver nanoparticles and the $[Ru(bpy)_3]^{2+}$ molecules, thus producing no SERS signal. Tables 2 and 3 present average integrated Raman intensities for the integrated band obtained for a sample of swabs using a 1.0 NDF and various laser powers (N = 6), and integrated Raman intensities for one laser power, respectively. These tables corroborate the plotted data indicating that lower concentrations produced greater integrated Raman intensities. The laser power at the samples were used for these calculations, i.e., the units cps/mW refers to the counts per second of Raman intensity normalized by laser power at the sample.

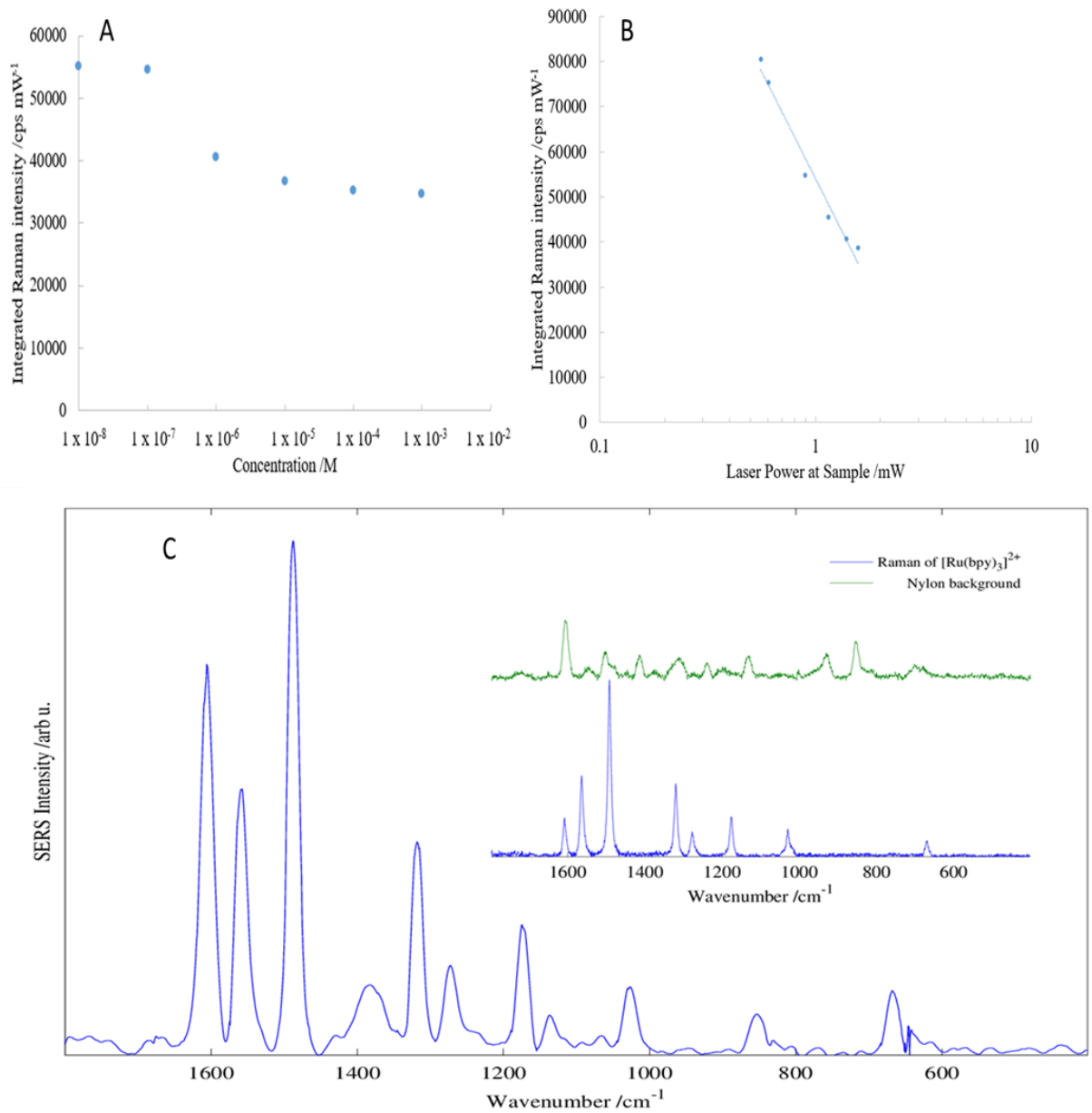

Figure 11. Summary of $[Ru(bpy)_3]^{2+}$ studies. (A) plot of integrated Raman intensity vs. concentration at 1.575 mW. (B) plot of integrated Raman intensity vs. laser power at sample. The line, best fit by least squares regression has the equation of I_{RI} = -41296ln(Lp) + 54053 cps mW^{-1} with a correlation coeffiecient of 0.9753. (C) SERS spectrum of 1 x 10^{-8} M $[Ru(bpy)_3]^{2+}$ with the Raman spectrum of $[Ru(bpy)_3]^{2+}$ and SERS background spectrum of nylon shown in the top right of the spectrum.

Table 2. Average integrated Raman intensity obtained through swabbing various concentrations of $[Ru(bpy)_3]^{2+}$ examined using multiple laser powers. Values are reported with a 95% confidence interval (95%, 6).

Swab /M of Rbpy	Average Integrated Raman Intensity x10^5 /(cps/mW)
1 x 10^{-3}	0.4 ± 0.1
1 x 10^{-4}	0.5 ± 0.1
1 x 10^{-5}	0.6 ± 0.2
1 x 10^{-6}	0.6 ± 0.1

Table 3. Integrated Raman intensities of various $[Ru(bpy)_3]^{2+}$ concentrations for a laserhead power of 100 mW.

Swab /M of Rbpy	Integrated Raman Intensity x 10^5 /(cps/mW)
1 x 10^{-3}	0.35
1 x 10^{-4}	0.35
1 x 10^{-5}	0.48
1 x 10^{-6}	0.46
1 x 10^{-7}	0.55
1 x 10^{-8}	0.55

4.4.3. Seminal fluid studies

Seminal fluid studies began by first attempting to obtain a Raman spectrum of semen to serve as both a comparison to a literature spectrum and a reference for future studies. However, a conventional Raman spectrum could not be obtained with the available instrumentation using the HeNe laser. The HeNe laser was chosen as the excitation source for SERS of seminal fluid as previous studies in the lab had obtained SERS of seminal fluid using that excitation wavelength. So they could be compared to the reference SERS spectrum obtained of seminal fluid, all seminal fluid spectra were collected using a 1 second acquisition time and 15 accumulations, and every Raman measurement involved finding the optimum focal plane for measurement by adjusting the stage to maximize signal to the detector. To acquire the initial SERS spectrum of seminal fluid using the swabs, a silver-modified swab was dipped into seminal fluid and analyzed immediately. The resulting SERS spectrum is shown in Figure 12.

The bands in the spectrum have been labeled to illustrate the correspondence to that of a literature Raman spectrum, in which bands and vibrational modes have been assigned based on data from other literature sources.[22] This band and vibrational mode assignment data is presented in Table 4.[22,51–65] Figure 13 shows the overlaid spectra of the seminal fluid SERS signal and nylon SERS signal that has been normalized. The SERS spectra of semen and nylon are similar as semen is a complicated mixture rich with proteins, and nylon is a synthetic protein. However, spectral comparison reveals differences, and the bands around 653 and 723 cm^{-1} can be used as indication for the presence of seminal fluid as they are absent in the nylon substrate. The band indicative of for choline (723 cm^{-1}), a constituent of a neurotransmitter present in semen, is especially significant as it's a unique chemical component to seminal fluid and has been used as a chemical identifier for the presence of semen in past forensic investigation techniques.[22,66]

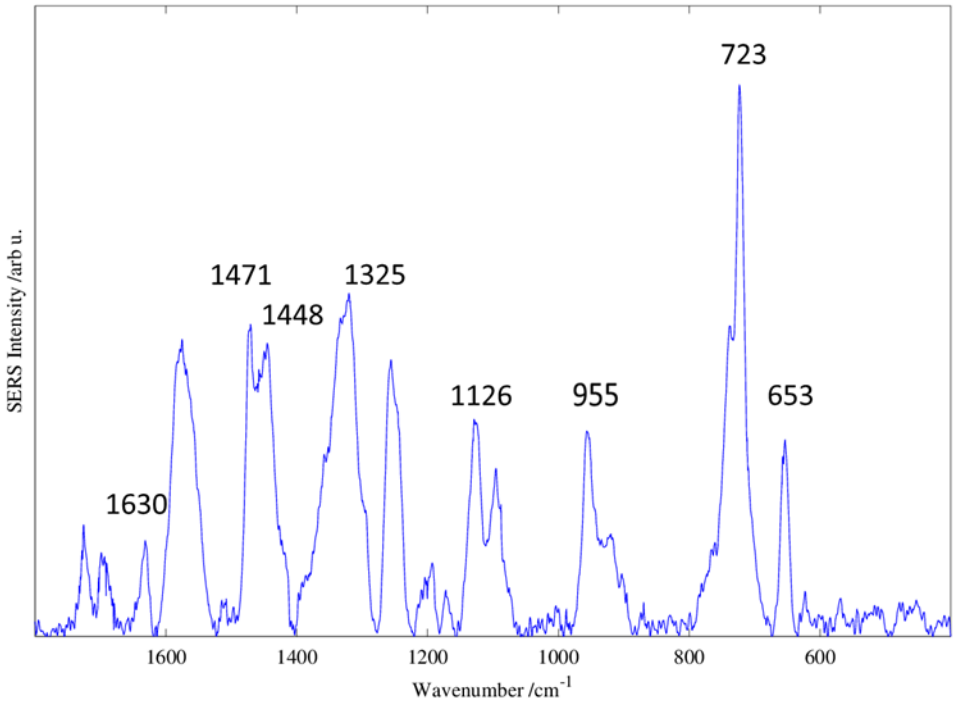

Figure 12. SERS spectrum of semen with labeled bands that overlap with a literature Raman vibrational mode assignment of semen.

Table 4. Literature Raman vibrational mode assignments of semen.

Raman Shift /cm^{-1}	Vibrational Mode
641	Ring deformation (Tyrosine)[52,53,61]
715	CN sym. stretching (Choline)[56–58]
829	Ring breathing (Tyrosine)[52,53,61]
958	PO_4^{3-} sym. Stretching (SPH)[22,60,63]
1125	CN asym. stretching (SPH)[22,59]
1179	CH_2/NH_3 rocking (Tyrosine)[52,53,61]
1265	Sym. ring deformation (Tyrosine)[52,53,64]
1327	Ring stretching (Tyrosine)[52,53,61]
1448	CH_2, CH_3 bend (Tryptophan)[51,54,55]
1461	CH_2 bending (SPH)[22,51]
1616	CC stretching (Tyrosine)[52,53,62]
1668	Amid I (Albumin)[54,55,65]

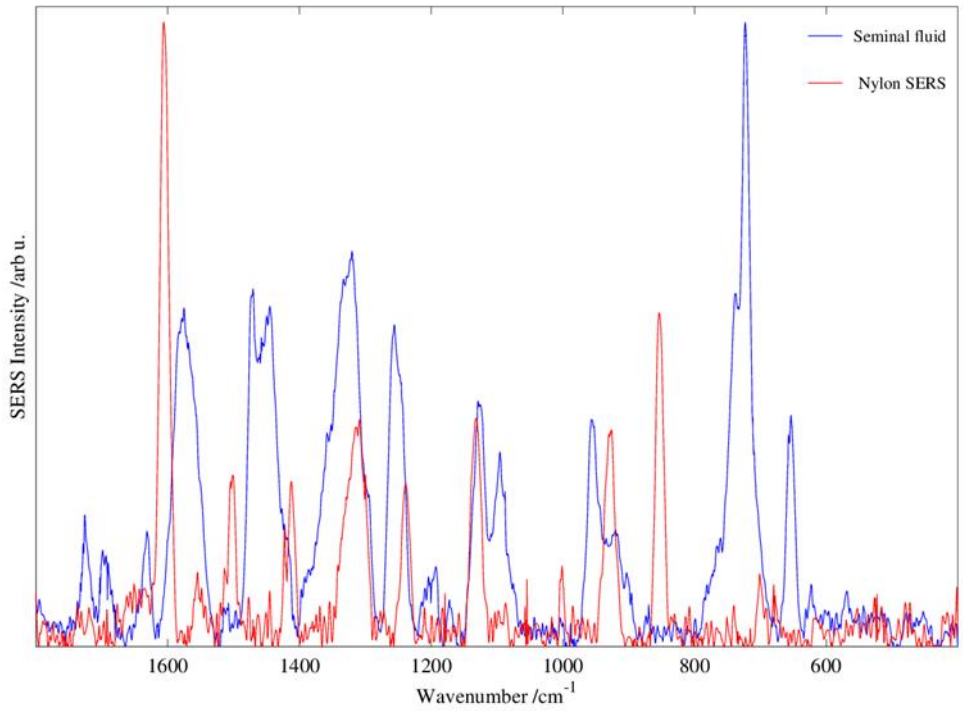

Figure 13. Seminal fluid and nylon SERS spectra overlaid for comparison.

Further seminal fluid studies included swabbing of dried (overnight) seminal fluid from a microscope slide to simulate swabbing from a hard surface as might be encountered at crime scenes. A representative SERS spectrum is shown in Figure 14 that has been normalized. As is shown in the figure, swabbing of seminal fluid from the microscope slide and its subsequent SERS spectrum are of good enough quality to distinguish semen and nylon. Investigations into the smallest volume of seminal fluid which would successfully give SERS signal was determined to be 12 µL and the resulting spectrum is shown in Figure 15, which has also been normalized. Additionally, seminal fluid was dried on a bed sheet overnight and swabbed in a similar manner. However, after swabbing the seminal fluid from the bed sheet no SERS signal was observed indicating problems with the transfer of seminal fluid from the sheet to the swab. The bed sheet visually appeared to have silver left behind from the swab presumably a result of the mechanical

friction from the swabbing motion. One plausible reason for this observation is that in addition to tightly bound particles, some are loosely bound during the synthesis and these loosely bound particles are what is observed on the sheet. Efforts to obtain signal while addressing this issue included doubling and tripling the volume of sample swabbed, wetting the sample and swabbing using a dry swab, laying the sheet on top of the swab and wetting the sheet with water from above the swab and lastly, swabbing until no more silver appeared to be coming off and subsequently attempting to obtain SERS signal. However, despite these efforts no SERS signal was obtained further indicating complications in the transfer of seminal fluid from the sheet.

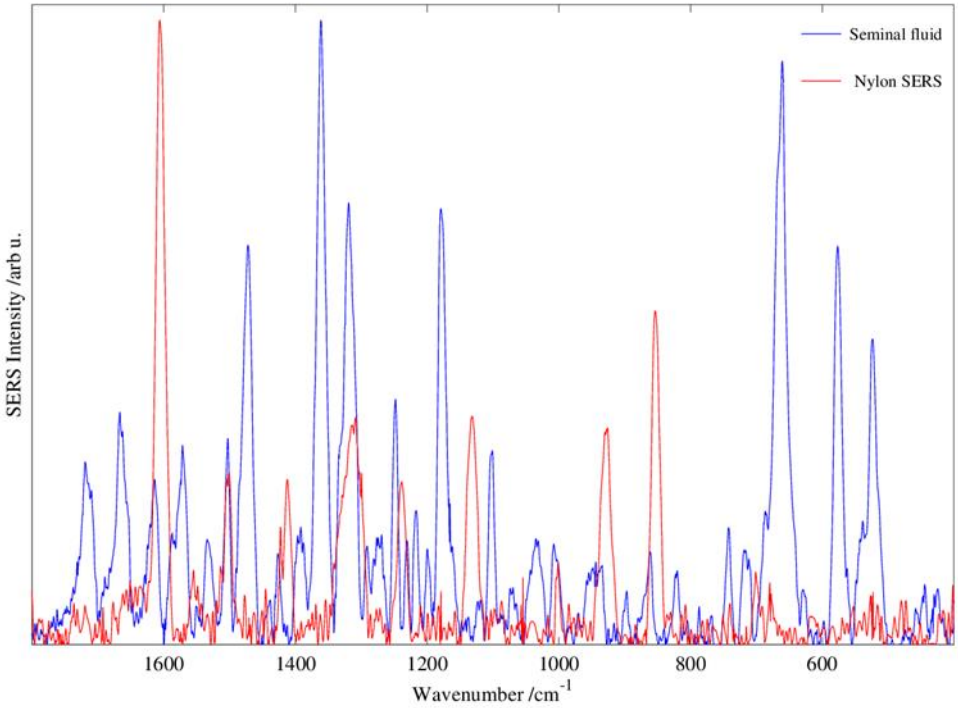

Figure 14. SERS spectrum of 100 µL of semen swabbed from a microscope slide after drying and stored in a freezer overlaid with the SERS nylon background.

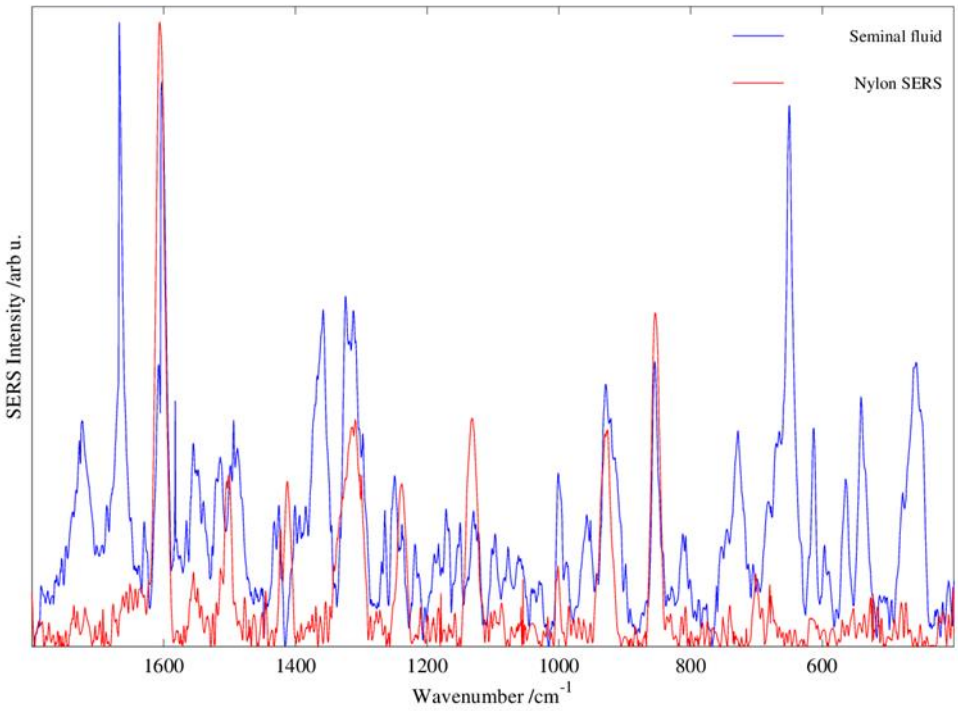

Figure 15. Overlaid spectra of 12 µL of semen with the SERS nylon background.

Throughout the seminal fluid studies, it was observed that SERS signal was difficult to obtain from dry samples. Wet samples with no drying time before analysis worked best for initial signal detection when swabs were analyzed at room temperature. Allowing the swabs to dry after initially detecting SERS signal would result in diminishment of the signal, as shown in Figure 16. As can be seen in the figure, the signal diminished greatly over the course of 20 minutes. In fact, only two bands are distinguishable after drying. Due to the presence of only these bands, the resulting spectrum does not resemble the SERS spectrum of nylon, but also cannot be confidently identified as seminal fluid. Such a change in the spectrum could arise from separation of the sample as it dries and is subsequently analyzed. Shown in Figure 17 is the spectrum of a swab stored at room temperature against the nylon background for visual comparison to the spectrum initially detected while the swab was wet in Figure 16. The spectra

of the SERS seminal fluid and nylon signal appear visually distinguishable and have been normalized to highlight such. Swabs that were stored at room temperature after swabbing the seminal fluid still produced signal, but was not as easily obtained and the signal was less intense.

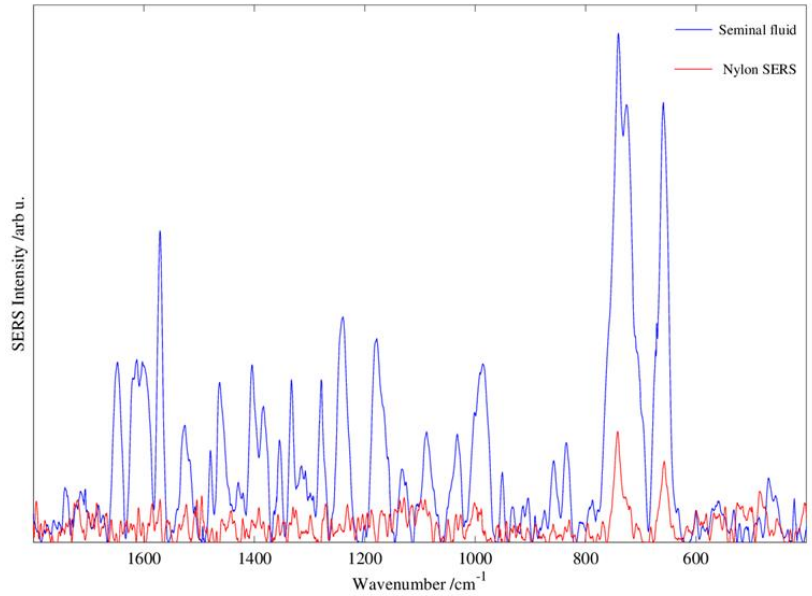

Figure 16. Overlaid spectra of a swab with 0 minutes of drying with the resulting spectrum after the swab was allowed a drying period of 20 minutes.

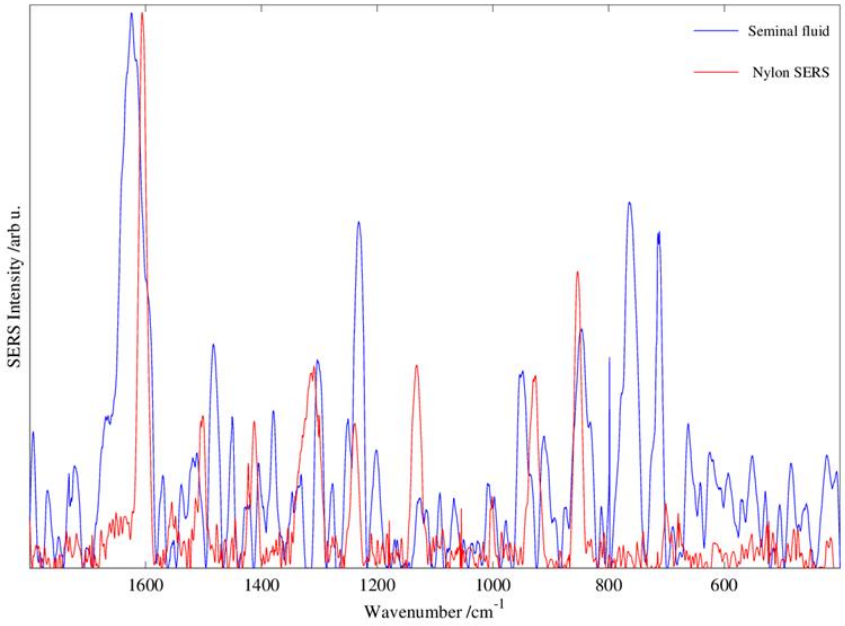

Figure 17. Overlaid spectra of seminal fluid sample analyzed at room temperature vs. the nylon background.

Despite the advantage of initial detection while the swabs were wet, the signal would diminish over time for reasons that could include, the sample was moving or the measurement process, i.e., exposure to the excitation laser, is degrading the sample by bond cleavages, either optically (by the laser)or thermally. If the bonds of the seminal fluid analyte molecules are not being broken optically this would indicate a thermal issue, as a result of choice of the laser excitation wavelength and thermal heating. Thermal heating could be a potential problem with the silver nanoparticles as they have been shown to release heat when interacting with an external electromagnetic field.[67] However, because the swabs are made of porous fibers, which would allow space between fibers to dissipate the heat produced by the laser, the swabs should act as an efficient heat sink. The heat sink property of the swabs would then aid in preventing thermal degradation of the sample.

Freezer storage of the swabs, after the swabbing of the seminal fluid and subsequently drying at room temperature, was experimentally determined to be the optimum storage method. Data that supports this conclusion was found when a swab, reanalyzed after being stored in the freezer at -15.3 °C, produced SERS signal that overlapped well with the literature Raman spectrum of semen. This freezer storage result showed that SERS signal was easy to obtain with good signal-to-noise ratios, despite the seminal fluid being dried prior to storage. The same case applies to Figure 14, in which the swab was measured four days after being stored in a freezer at the same temperature. Freezer storage may increase the efficiency of the heat sink property of the swab, as compared to room temperature storage. This allows the swab to be cold at the onset of measurements which can potentially prevent degradation of the sample allowing greater chance of obtaining SERS signal.

Analysis of this hypothesis is shown in Figure 18 in which the spectra have been normalized. As can be seen in the figure, allowing the swab to come to room temperature resulted in weakening of the semen SERS signal. Storing the swab back in the freezer and subsequently reanalyzing, however, resulted in better SERS signal and intensity though a different spot was analyzed. Likewise, a visual difference can be seen in the semen SERS signal resulting from difficulty in measuring the same spot once the swab has been moved. Figure 19 further highlights this heterogeneity as four different spots were analyzed on the same swab. The four spectra have visual similarities, such as the band unique to choline around 723 cm^{-1}, but also have differences, highlighting that different locations of analyzed sample affects the resulting spectrum, even though the spots were all on the same swab.

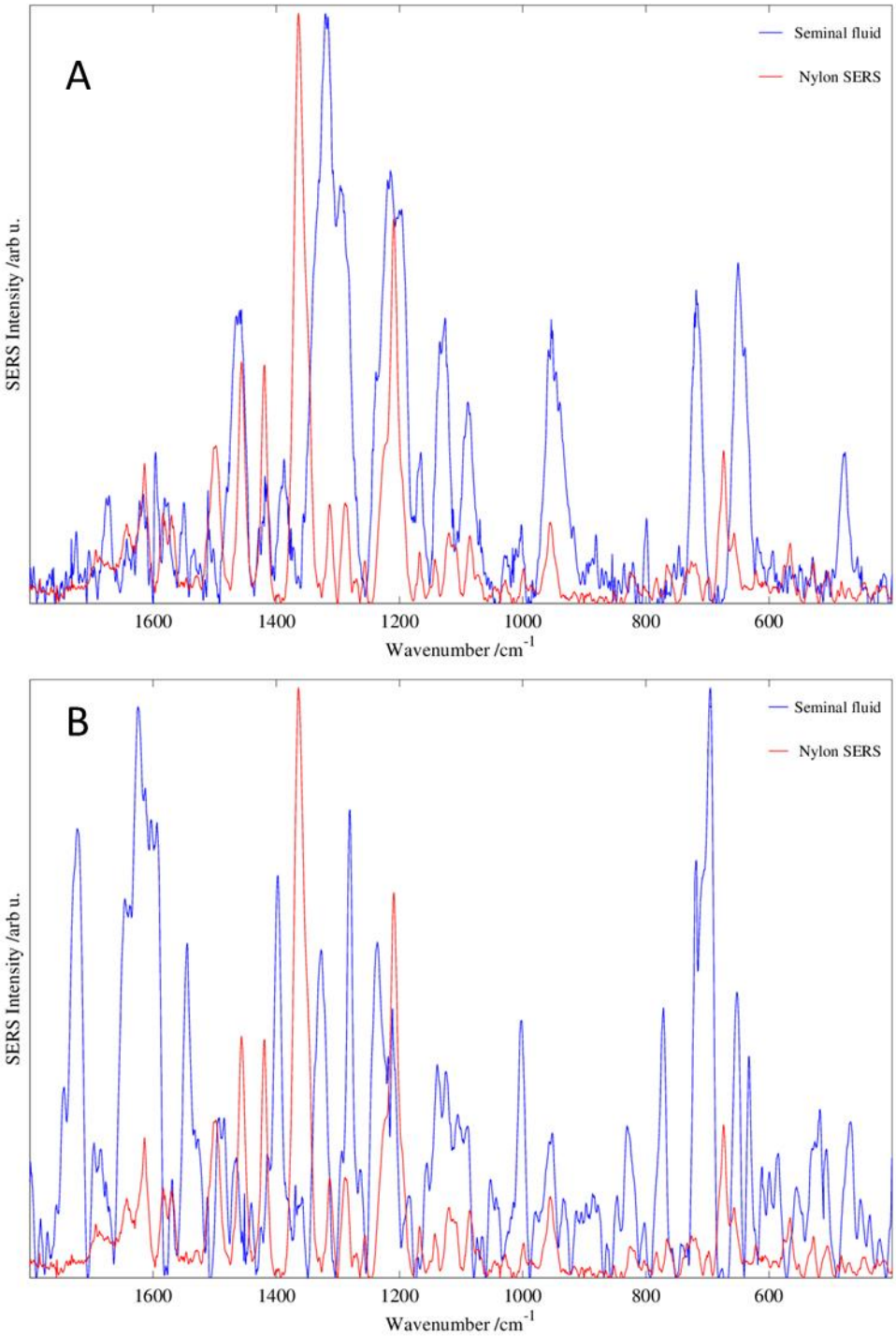

Figure 18. Spectra acquired from freezer studies. (A) overlaid spectra of a swab analyzed after being stored in the freezer with the resulting spectrum of allowing the swab to come to room temperature. (B) overlaid spectra of room temperature spectrum from (A) with resulting spectrum after storing the swab back in the freezer and subsequently reanalyzing.

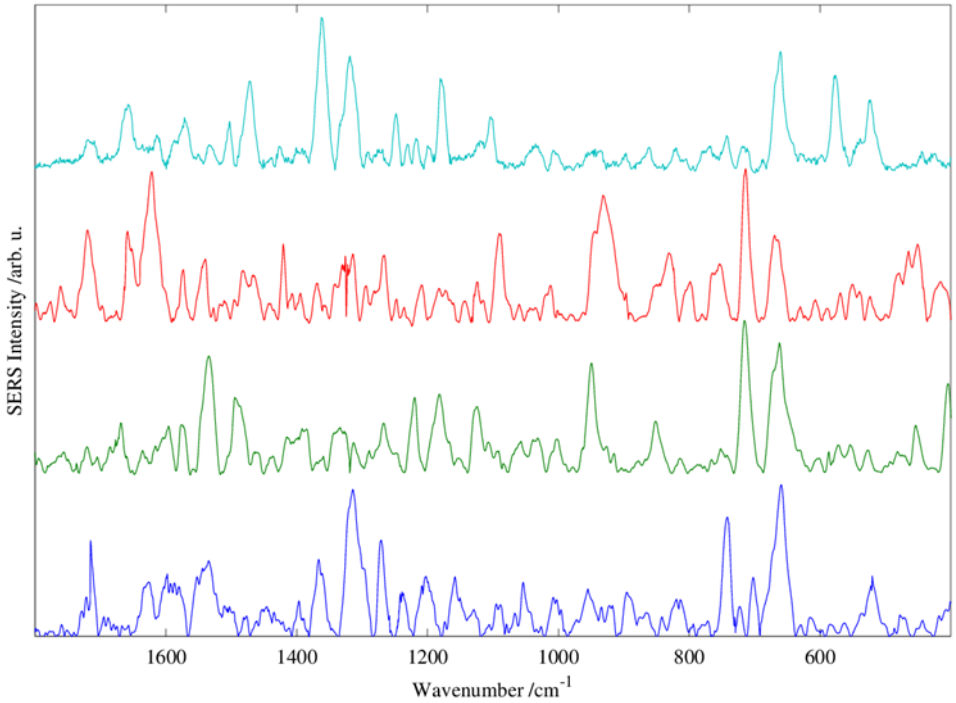

Figure 19. Stacked spectra of dried semen analyzed on one swab at four different locations.

SERS is a sensitive technique, making it promising for many areas of research. However, SERS measurements can be prone to poor reproducibility as result of non-controllable interaction of analyte molecules with the SERS substrates. To overcome the issue of reproducibility, a wider laser beam could be used to analyze a greater surface area of the swab. Another method would be to collect spectra at different points and obtain an average spectrum. Also, by focusing on a band that represents the vibrational mode of a constituent unique to semen during analysis, such as the band responsible for choline appearing at approximately 723 cm^{-1} and present in all four spectra in Figure 19, could aid in the reproducibility. Future work on this project will be focused on overcoming some of the limitations experienced as the research progressed. The following discussion highlights some of the potential causes for the lack of reproducibility. Over the course of the research, it was observed that the dominant bands of the seminal fluid spectrum would shift in dimensions of both left/right. This poor

reproducibility could arise from the following factors: the seminal fluid is a complex and heterogeneous mixture and the swabs are further increasing this heterogeneity, or because of the degree of dryness of the sample. The increase in heterogeneity is due to the swabs containing random hot spots which are distributed across them as a result of the sporadic silver nanoparticle attachment. Since a dry sample is being measured, the degree of dryness/chemisorption of the molecules contained within the seminal fluid on the silver nanoparticles results in structural changes. Given the sensitivity of SERS measurements, it is possible that these structural changes resulting from the solvation of the seminal fluid, and the effect of separation of the sample are being recorded in the evolving spectra.

CHAPTER 5. CONCLUSIONS AND FUTURE WORK

The hydrogen reduction method for synthesizing silver nanoparticles was modified for attachment of the nanoparticles to fibers of commercially available nylon swabs. The resulting silver-modified swabs have been assessed by ICP-OES, electron microscopy and Raman spectroscopy for silver nanoparticle coverage and the use of SERS. The swabs have been shown to provide SERS enhancements using two model dye compounds, and seminal fluid for forensic applications. The analysis of the swabs via ICP-OES and electron microscopy revealed that the silver nanoparticles are sporadically distributed across the nylon fibers.

This research provides evidence that silver nanoparticles synthesized via the hydrogen reduction method can be attached to fibers of commercially available nylon swabs that can ultimately serve as a collection medium facilitating analysis by SERS as a non-destructive confirmatory method of detection of seminal fluid. This collection/medium interface holds significance as risk of exogenous DNA contamination would be greatly reduced if suspected evidentiary samples were collected directly onto the measurement platform. Different swabbing scenarios were explored throughout this research in attempts to simulate forensic swabbing and explore methods to yield the highest SERS intensity. These explorations found that fluorescence can be a challenge to overcome in order to obtain useful SERS signal, but that the swabs provide significant SERS enhancements once fluorescence is quenched. Throughout the research, it was observed that SERS signal was more easily obtained when the swabs were still wet from the swabbing process. This was true for lower concentrations of $[Ru(bpy)_3]^{2+}$ (≤ 1 µM), and especially true for seminal fluid. During the seminal fluid studies, it was observed that the Raman signal diminished as the swab dried. Swabs that were stored in the freezer however,

allowed useful SERS signal to be obtained, regardless of degree of dryness prior to freezer storage, and thus was concluded to be the best storage method.

Future research will need to be performed in order to achieve more systematic coverage of nanoparticles on the fibers of the swabs. Throughout this research, it was determined that the addition of the swabs to the reaction slowed the reaction, resulting in smaller nanoparticles than are typically produced via the hydrogen reduction method. As a result of such sporadic coverage, difficulty arose in obtaining useful SERS signal distinguishable from that of fluorescence. The benefit of a more systematic coverage is that the swabs would provide better Raman signal than fluorescence, ultimately leading to better SERS enhancements. Once more systematic coverage is achieved, either by chemical pre-treatment of the swabs, plasma cleaning of the swabs before the synthesis or altering reaction conditions, further studies could be performed on the SERS enhancements produced by the swabs. Investigations of concentrations below 1×10^{-8} M $[Ru(bpy)_3]^{2+}$ will be explored as lower concentrations have previously been detected using the same instrumentation.

Other experiments to be performed as part of future work include examining how much silver is being left behind following the swabbing of a soft surface. This will be accomplished by performing ICP-OES of the sheets after swabbing. Likewise, efforts to prevent the silver from being left behind on soft surfaces will also need to be explored. One option would to be to heat the swabs via a steam treatment to serve as an annealing process for the nanoparticles which would simultaneously increase the robustness of the swabs.[33] Another option would be to incorporate a polymer, such as PDDA, which has been used to immobilize silver nanoparticles for SERS studies.[44,65] Efforts to maximize the amount of seminal fluid transferred from a soft surface will also need to be explored in order for the swabs to have full potential for forensic

applications. An option for this would be to take a cutting of the soft surface material with the seminal fluid stain, placing it in a phosphate-buffered saline (PBS) solution with a pH of 7.4 in a shaking incubator, dipping the swab in this solution and allowing it to dry before being measured. This would serve as an extraction process that would allow more seminal fluid to be transferred to the swab. Another option to enhance the extraction of the seminal fluid from the sheet would be to use organics, such as glycerol, which has been shown to interact with proteins, to better solvate the seminal fluid, thus leading to better transfer to the swab.

With the possibility of optical degradation of the sample, future work could include accounting and correcting for such degradation. Optical degradation could be corrected using a longer wavelength excitation than the HeNe laser. Many authors presenting Raman investigations of bodily fluids have done so using a NIR 785 nm wavelength excitation. However, SERS enhancements would decrease as a result of this new excitation wavelength due to SERS enhancements being inversely proportional to excitation wavelength.

CHAPTER 6. REFERENCES

(1) Kayser, M.; de Knijff, P. Improving Human Forensics through Advances in Genetics, Genomics and Molecular Biology. *Nat. Rev. Genet.* **2012**, *13* (10), 753–753.

(2) Virkler, K.; Lednev, I. K. Analysis of Body Fluids for Forensic Purposes: From Laboratory Testing to Non-Destructive Rapid Confirmatory Identification at A Crime Scene. *Forensic Sci. Int.* **2009**, *188* (1-3), 1–17.

(3) Brownlow, R. J.; Dagnall, K. E.; Ames, C. E. A Comparison of DNA Collection and Retrieval from Two Swab Types (Cotton and Nylon Flocked Swab) When Processed Using Three QIAGEN Extraction Methods. *J. Forensic Sci.* **2012**, *57* (3), 713–717.

(4) Mozayani, A.; Noziglia, C. *Forensic Laboratory Handbook: Procedures and Practice*, First.; Humana Press: New York, 2005.

(5) Saferstein, R. *Forensic Science: From the Crime Scene to the Crime Lab*, First.; Anthony, V. R., Peyton, T., Kelly, A., Eds.; Pearson Prentice Hall: Upper Saddle River, 2013.

(6) Greenfield, A.; Sloan, M. M. Identification of Biological Fluids and Stains. In *Forensic Science: An Introduction to Scientific and Investigative Techniques, Fourth Edition*; James, S. H., J., N., Eds.; CRC Press: Boca Raton, 2003; pp 203–220.

(7) *Forensic Science: An Introduction to Scientific and Investigative Techniques*; James, S. H., Nordby, J. J., Eds.; CRC Press: Boca Raton, 2003.

(8) Watson, N. *The Analysis of Body Fluids, Crime Scene to Court; the Essentials of Forensic Science*, second.; White, P. C., Ed.; Royal Society of Chemistry: Cambridge, UK, 2004.

(9) Ball, D. W. *Physical Chemistry*, Second.; Lockwood, L., Ed.; Cengage Learning: Stamford, 2014.

(10) Larkin, P. *IR and Raman Spectroscopy*; Elsevier: Amsterdam, 2011.

(11) Smith, E.; Dent, G. *Modern Raman Spectroscopy: A Practical Approach*, 1st ed.; J. Wiley: Hoboken, 2005.

(12) Ferraro, J. R.; Nakamoto, K.; Brown, C. W. *Introductory Raman Spectroscopy*, Second.; Academic Press: San Diego, 2003.

(13) Ford, S. M. *Modern Instrumental Analysis*; Comprehensive Analytical Chemistry; Elsevier, 2006; Vol. 47.

(14) Stamplecoskie, K. G.; Scaiano, J. C.; Tiwari, V. S.; Anis, H. Optimal Size of Silver Nanoparticles for Surface-Enhanced Raman Spectroscopy. *J. Phys. Chem. C* **2011**, *115* (5), 1403–1409.

(15) Bell, S. *Forensic Chemistry*, Second.; Jaworski, A., Zalesky, J., Eds.; Pearson Prentice Hall: Upper Saddle River, 2013.

(16) Triplett, J. S.; Hatfield, J. A.; Kaeff, T. L.; Ramsey, C. R.; Robinson, S. D.; Standifer, A. F. Raman Spectroscopy as a Simple, Rapid, Nondestructive Screening Test for Methamphetamine in Clandestine Laboratory Liquids. *J. Forensic Sci.* **2013**, *58* (6).

(17) Tănase, I. G.; Udrıştioiu, F. M.; Bunaciu, A. a.; Aboul-Enein, H. Y. Application of Micro-Raman and FT - IR Spectroscopy in Forensic Analysis of Questioned Documents. *Appl. Spectrosc. Rev.* **2012**, *47* (6), 484–494.

(18) Suzuki, E. M.; Carrabba, M. In Situ Identification and Analysis of Automotive Paint Pigments Using Line Segment Excitation Raman Spectroscopy: I. Inorganic Topcoat Pigments. *J. Forensic Sci.* **2001**, *46* (5), 1053–1069.

(19) Was-gubala, J.; Machnowski, W. Application of Raman Spectroscopy for Differentiation Among Cotton and Viscose Fibers Dyed with Several Dye Classes. *Spectrosc. Lett.* **2014**,

47 (7), 527–535.

(20) Hendra, P. J.; Watson, D. S.; Cudby, M. E. A.; Willis, H. A.; Holliday, P. The Laser-Raman Spectra of Some Nylons. *J. Am. Chem. Soc. D Chem. Commun.* **1970**, No. 17.

(21) Virkler, K.; Lednev, I. K. Raman Spectroscopy Offers Great Potential for the Nondestructive Confirmatory Identification of Body Fluids. *Forensic Sci. Int.* **2008**, *181* (1-3), 1–5.

(22) Virkler, K.; Lednev, I. K. Raman Spectroscopic Signature of Semen and Its Potential Application to Forensic Body Fluid Identification. *Forensic Sci. Int.* **2009**, *193* (1-3), 56–62.

(23) Sharma, B.; Frontiera, R.; Henry, A.; Ringe, E.; Van Duyne, R. SERS: Materials, Applications, and the Future. *Mater. Today* **2012**, *15* (1-2), 16–25.

(24) Douketis, C.; Haslett, T. L.; Wang, Z.; Moskovits, M.; Iannotta, S. Self-Affine Silver Films and Surface-Enhanced Raman Scattering: Linking Spectroscopy to Morphology. *J. Chem. Phys.* **2000**, *113* (24), 11315–11323.

(25) *Nanophotonics with Surface Plasmons*, First.; Shalaev, V. M., Kawata, S., Eds.; Elsevier: Amsterdam, 2007.

(26) Aroca, R. *Surface-Enhanced Vibrational Spectroscopy*; John Wiley & Sons Ltd.: West Sussex, 2006.

(27) Lombardi, J. R.; Birke, R. L.; Lu, T.; Xu, J. Charge Transfer Theory of Surface-Enhanced Raman Spectroscopy: Herzberg-Teller Contributions. *J. Chem. Phys.* **1986**, *84*, 4174–4180.

(28) Muehlethaler, C.; Leona, M.; Lombardi, J. R. Review of Surface Enhanced Raman Scattering Applications in Forensic Science. *Anal. Chem.* **2016**, *88* (1), 152–169.

(29) Boyd, S.; Bertino, M. F.; Ye, D.; White, L. S.; Seashols, S. J. Highly Sensitive Detection of Blood by Surface Enhanced Raman Scattering. *J. Forensic Sci.* **2013**, *58* (3), 753–756.

(30) *Resonance Raman Spectroscopy as an Analytical Tool*; Melveger, A. J., Ed.; Franklin Institute Press: Philadelphia, 1978.

(31) Evanoff, D. D.; Chumanov, G. Synthesis and Optical Properties of Silver Nanoparticles and Arrays. *ChemPhysChem* **2005**, *6* (7), 1221–1231.

(32) Rycenga, M.; Cobley, C. M.; Jie, Z.; Weiyang, L.; Moran, C. H.; Qiang, Z.; Dong, Q.; Younan, X. Controlling the Synthesis and Assembly of Silver Nanostructures for Plasmonic Applications. *Chem. Rev.* **2011**, *111* (6), 3669–3712.

(33) Zhang, G.; Liu, Y.; Gao, X.; Chen, Y. Synthesis of Silver Nanoparticles and Antibacterial Property of Silk Fabrics Treated by Silver Nanoparticles. *Nanoscale Res. Lett.* **2014**, *9* (1), 216–224.

(34) Brogliato, A. R.; Borges, P. A.; Barros, J. F.; Lanzetti, M.; Valenca, S.; Oliveria, N. C.; Izário-Filho, H. J.; Benjamin, C. F. The Effect and Safety of Dressing Composed by Nylon Threads Covered With Metallic Silver in Wound Treatment. *Int. Wound J.* **2014**, *11* (2), 190–197.

(35) Wright, J. B.; Lam, K.; Burrell, R. E. Wound Management in an Era of Increasing Bacterial Antibiotic Resistance: A Role for Topical Silver Treatment. *Am. J. Infect. Control* **1998**, *26* (6), 572–577.

(36) Ip, M.; Lui, S. L.; Poon, V. K. M.; Lung, I.; Burd, A. Antimicrobial Activities of Silver Dressings: An in Vitro Comparison. *J. Med. Microbiol.* **2006**, *55*, 59–63.

(37) Abedini, F.; Ahmadi, A.; Yavari, A.; Hosseini, V.; Mousavi, S. Comparison of Silver Nylon Wound Dressing and Silver Sulfadiazine in Partial Burn Wound Therapy. *Int.*

Wound J. **2013**, *10* (5), 573–578.

(38) Kelly, F. M.; Johnston, J. H. Colored and Functional Silver Nanoparticle À Wool Fiber Composites. **2011**, 1083–1092.

(39) Tang, B.; Zhang, M.; Hou, X.; Li, J.; Sun, L.; Wang, X. Coloration of Cotton Fibers with Anisotropic Silver Nanoparticles. *Ind. Eng. Chem. Res.* **2012**, *51* (39), 12807–12813.

(40) Lu, Z.; Xiao, J.; Wang, Y.; Meng, M. In Situ Synthesis of Silver Nanoparticles Uniformly Distributed on Polydopamine-Coated Silk Fibers for Antibacterial Application. *J. Colloid Interface Sci.* **2015**, *452*, 8–14.

(41) Lu, Z.; Meng, M.; Jiang, Y.; Xie, J. UV-Assisted in Situ Synthesis of Silver Nanoparticles on Silk Fibers for Antibacterial Applications. *Colloids Surfaces A Physicochem. Eng. Asp.* **2014**, *447*, 1–7.

(42) Li, R.; He, M.; Li, T.; Zhang, L. Preparation and Properties of Cellulose/silver Nanocomposite Fibers. *Carbohydr. Polym.* **2015**, *115*, 269–275.

(43) Dong, H.; Fey, E.; Gandelman, A.; Jones, W. E. Synthesis and Assembly of Metal Nanoparticles on Electrospun Poly (4-Vinylpyridine) Fibers and Poly (4-Vinylpyridine) Composite Fibers. *Chem. Mater.* **2011**, No. 16, 2008–2011.

(44) Montazer, M.; Nia, Z. K. Conductive Nylon Fabric Through in Situ Synthesis of Nano-Silver: Preparation and Characterization. *Mater. Sci. Eng. C* **2015**, *56*, 341–347.

(45) Meng, M.; He, H.; Xiao, J.; Zhao, P.; Xie, J.; Lu, Z. Controllable in Situ Synthesis of Silver Nanoparticles on Multilayered Film-Coated Silk Fibers for Antibacterial Application. *J. Colloid Interface Sci.* **2016**, *461*, 369–375.

(46) Mirjalili, M.; Yaghmaei, N.; Mirjalili, M. Antibacterial Properties of Nano Silver Finish Cellulose Fabric. *J. Nanostructure Chem.* **2013**, *3* (43).

(47) Chen, Y.-H.; Hsu, C.-C.; He, J.-L. Antibacterial Silver Coating on Poly(ethylene Terephthalate) Fabric by Using High Power Impulse Magnetron Sputtering. *Surf. Coatings Technol.* **2013**, *232*, 868–875.

(48) Evanoff, D. D.; Chumanov, G. Size-Controlled Synthesis of Nanoparticles. 1. "Silver-Only" Aqueous Suspensions via Hydrogen Reduction. *J. Phys. Chem.* **2004**, *108* (37), 13948–13956.

(49) Li, Z.; Qian, X.-F.; Yin, J.; Zhu, J. Y. A Simple Method for Selective Immobilization of Silver Nanoparticles. *Appl. Surf. Sci.* **2005**, *250* (1-4), 109–116.

(50) Kalishwaralal, K.; BarathManiKanth, S.; Pandian, S. R. K.; Deepak, V.; Gurunathan, S. Silver Nanoparticles Impede the Biofilm Formation by Pseudomonas Aeruginosa and Staphylococcus Epidermidis. *Colloids Surfaces B Biointerfaces* **2010**, *79* (2), 340–344.

(51) Grasselli, J. *Chemical Applications of Raman Spectroscopy*; John Wiley & Sons: New York, 1981.

(52) Kiefer, W.; Mazzolini, A. P.; Stoddart, P. R. Reference Database of Raman Spectra of Biological Molecules. *J. Raman Spectrosc.* **2007**, *38* (April), 1538–1553.

(53) Johnson, C. R.; Ludwig, M.; Asher, S. a. Ultraviolet Resonance Raman Characterization of Photochemical Transients of Phenol, Tyrosine, and Tryptophan. *J. Am. Chem. Soc.* **1986**, *108* (5), 905–912.

(54) Liang, J.; Cheng, Y.; Han, H. Study on the Interaction between Bovine Serum Albumin and CdTe Quantum Dots with Spectroscopic Techniques. *J. Mol. Struct.* **2008**, *892* (1-3), 116–120.

(55) Ivanov, A. I.; Zhbankov, R. G.; Korolenko, E. A.; Korolik, E. V.; Meleshchenko, L. A.; Marchewka, M.; Ratajczak, H. Infrared, Raman Spectroscopic Studies of the Structure of

Human Serum Albumin under Various Ligand Loads. *J. Appl. Spectrosc.* **1994**, *60* (5), 305–309.

(56) Edsall, J. Raman Spectra of Amino Acids and Related Compounds. VI. Sarcosine, Ethanolamine, Choline, Betaine and Betaine Derivatives. *J. Am. Chem. Soc.* **1943**, *2833* (8), 1767–1770.

(57) Koyama, Y.; Toda, S. Raman Spectra and Conformation of the Glycerophosphorylcholine Headgroup. *Chem. Phys. Lipids* **1977**, *19* (1), 74–92.

(58) Spiker, R. J.; Levin, I. Raman Spectra and Vibrational Assignments for Dipalmitoyl Phosphatidylcholine and Structurally Related Molecules. **1975**, *388* (3), 361–373.

(59) Bertoluzza, A.; Fagnano, C.; Finelli, P.; Morelli, M. A.; Simoni, R.; Tosi, R. Raman and Infrared Spectra of Spermidine and Spermine and Their Hydrochlorides and Phosphates as a Basis for the Study of the Interactions between Polyamines and Nucleic Acids. *J. Raman Spectrosc.* **1983**, *14* (6), 386–394.

(60) Eapen, A.; Joe, I. H.; Aruldhas, G. Vibrational and SERS Spectra of Spermine Phosphate Hexahydrate. *Spectrosc. Lett.* **1997**, *30* (4), 751–770.

(61) Guicheteau, J.; Argue, A. H.; M. Jacobson, S. D. C. Raman and Surface-Enhanced Raman Spectroscopy of Amino Acids and Nucleotide Bases for Target Bacterial Vibrational Mode Identification. *Proc. SPIE* **2006**, No. 6281, 1–11.

(62) Stewart, S.; Fredericks, P. . Surface-Enhanced Raman Spectroscopy of Amino Acids Adsorbed on an Electrochemically Prepared Silver Surface. *Spectrochim. Acta Part A Mol. Biomol. Spectrosc.* **1999**, *55* (7-8), 1641–1660.

(63) Aza, P. N. de; Santos, C.; Pazo, A.; Aza, S. de; Cusco, R.; Artús, L. Vibrational Properties of Calcium Phosphate Compounds. 1 . Raman Spectrum of B-Tricalcium Phosphate.

Chem. Mater. **1997**, *9* (10), 912–915.

(64) Ludwig, M.; Asher, S. A. Ultraviolet Resonance Raman Excitation Profiles of Tyrosine: Dependence of Raman Cross Sections on Excited-State Intermediates. *J. Am. Chem. Soc.* **1988**, *110* (4), 1005–1011.

(65) Biological Applications of Raman Spectroscopy; Gremlich, H. U., Yan, B., Eds.; Marcel Dekker, Inc.: New York, 2001.

(66) Newsholme, E.; Leech, T. *Functional Biochemistry in Health and Disease*; Board, M., Ed.; Wiley-Blackwell: West Sussex, 2009.

(67) Govorov, A. O.; Richardson, H. H. Generating Heat with Metal Nanoparticles. *nanotoday* **2007**, *2* (1), 30–38.

(68) Daniels, J. K.; Chumanov, G. Nanoparticle-Mirror Sandwich Substrates for Surface-Enhanced Raman Scattering. *J. Phys. Chem. B* **2005**, *109* (38), 17936–17942.